Wang H, Blocken B, Lin Z. 2025. CFD simulation of the stratified atmospheric boundary layer: consistency between Monin-Obukhov similarity theory and the standard k-e model. Building and Environment: Art. 112284 https://doi.org/10.1016/j.jbuildenv.2024.112284

CFD simulation of the stratified atmospheric boundary layer: consistency between Monin-Obukhov similarity theory and the standard *k-ε* model

Hao (Simone) Wang [a,*], Bert Blocken [b,c], Zhang Lin [a]

[a] Department of Architecture and Civil Engineering, City University of Hong Kong, Hong Kong, China
[b] Institute of Mechanical, Process and Energy Engineering, Heriot-Watt University, Edinburgh, Scotland, United Kingdom
[c] Building Physics and Sustainable Design, Department of Civil Engineering, KU Leuven, Leuven, Belgium

*Corresponding author: Hao (Simone) Wang
Email: hwang666@cityu.edu.hk
Tel: +852 97846642

Highlights:

- The reason for the inhomogeneous ABL is theoretically investigated.
- A new model coefficient is proposed for the standard *k-ε* turbulence model.
- Horizontal homogeneity is maintained for both neutral and non-neutral ABL.
- The proposed solution is evaluated by modeling the stratified ABL around a building.

Abstract

Including thermal stratification in CFD simulations of the atmospheric boundary layer (ABL) flow is important for a wide range of applications, from pollutant dispersion over wind energy farm performance to urban thermal microclimate. One of the most important prerequisites for accurate CFD simulations of thermally stratified ABL flow is horizontal homogeneity. Horizontal homogeneity refers to the absence of unintended streamwise gradients

in the approach-flow profiles of mean velocity, turbulence quantities and temperature when flowing from the inlet of the domain to the location of interest in the domain, over uniformly rough level terrain. This paper proposes a generic and consistent solution to maintain horizontal homogeneity in CFD simulations of Monin-Obukhov similarity theory (MOST) based stratified ABL flow. A new description is proposed for the coefficient $C_{\varepsilon 3}$, which appears in the buoyancy term in the transport equation of the turbulence dissipation rate. This proposed solution is successfully demonstrated by simulations in an empty domain for four stability conditions ($1/L$ = 1/152.4 m^{-1}, 1/1071.7 m^{-1}, 0 m^{-1} and -1/296.3 m^{-1}), where the standard k-ε turbulence model with the new $C_{\varepsilon 3}$ is shown to well maintain the profiles of U, ε and T with only minor deviations for the k profiles. The performance of the turbulence model with the new $C_{\varepsilon 3}$ is also illustrated by the flow around a rectangular building under thermal stratification.

Keywords: Atmospheric boundary layer flow; Monin–Obukhov similarity theory; Thermal stratification; Horizontal homogeneity; Standard k-ε turbulence model; Computational fluid dynamics

Nomenclature

C_p	thermal capacity of air (= 1006.43) ($Jkg^{-1}K^{-1}$)
$C_{\varepsilon 1}$	constant in the standard k-ε turbulence model (= 1.44) (-)
$C_{\varepsilon 2}$	constant in the standard k-ε turbulence model (= 1.92) (-)
C_μ	constant in the standard k-ε turbulence model (= 0.09) (-)
g	gravitational acceleration (= 9.81) (ms^{-2})
G_k	production of turbulence kinetic energy due to mean velocity gradients ($kgm^{-1}s^{-3}$)
G_b	production of turbulence kinetic energy due to buoyancy ($kgm^{-1}s^{-3}$)
H	building height (= 100) (m)
H_{Domain}	domain height (m)
k	turbulent kinetic energy (m^2s^{-2})
ε	turbulent dissipation rate (m^2s^{-3})
k_s	equivalent sand-grain roughness height (m)

C_s	roughness constant (-)
k_S^+	dimensionless equivalent sand-grain roughness height (-)
L	Monin-Obukhov length (m)
L_{Domain}	domain length (m)
Pr_t	turbulent Prandtl number (= 0.85) (-)
$\dot{q}_0$	convective heat flux at the ground surface (Wm^{-2})
Re	Reynolds number (-)
Ri	Richardson number (-)
Sc_t	turbulent Schmidt number (= 0.70) (-)
S_{ij}	strain rate tensor (s^{-1})
T_{inlet}	temperature profile at the inlet (K)
T_0	near-ground air temperature (K)
u_*	friction velocity (ms^{-1})
u_j	fluctuating velocity components (u, v, w, j = 1, 2, 3) (ms^{-1})
U_{ref}	reference velocity (ms^{-1})
U_j	time-averaged velocity components (U, V, W, j = 1, 2, 3) (ms^{-1})
x, y, z	spatial coordinates in stream-wise (m), span-wise (m) and vertical directions (m)
z_0	aerodynamic roughness length (m)
θ_*	scaling temperature (K)
κ	von Karman constant (= 0.4186) (-)
μ_t	turbulent viscosity ($kgm^{-1}s^{-1}$)
σ_k	constant in the standard k-ε turbulence model (= 1.0) (-)
σ_ε	constant in the standard k-ε turbulence model (= 1.3) (-)
ρ	air density (kgm^{-3})
υ	kinematic molecular viscosity (m^2s^{-1})

ϕ_m integrated form of the similarity function (-)

ϕ_ε integrated form of the similarity function (-)

Ψ_m integrated form of the similarity function (-)

1. Introduction

Thermal stratification in the atmospheric boundary layer (ABL) refers to temperature and density gradients with height. The associated ABL can be classified as unstable, neutral or stable. Thermal stratification in the ABL can strongly affect the vertical distribution of mean velocity and turbulence quantities. As such, it is of importance for various applications, from pollutant dispersion over wind farm performance to urban thermal microclimate [1,2].

Turbulence is generally enhanced in unstable conditions and suppressed in stable conditions. For example, for plume dispersion from an isolated stack, the effluent plume can exhibit fanning with little vertical spread in stable conditions, whereas, in unstable conditions, vertical spreading can be so pronounced that the pollutant reaches ground level [3]. The negative influence of thermal stratification in terms of air pollution is evident in wintertime, when pollutant dispersion tends to be constrained by stable thermal stratification or thermal inversion [4]. Thermal stratification can also substantially impact wind farm performance, where the channelling or wake decay brought about by stable thermal stratification may lower the energy production [5]. Stable stratification also amplifies the nocturnal urban heat island effect [6], which refers to the higher air temperature in urban areas compared to their rural counterparts.

The thermal stratification in the ABL can be described based on the Monin–Obukhov similarity theory (MOST), in which the Monin-Obukhov length L (hereafter referred to as MO length) is used to indicate the extent of the stability [7-10]:

$$L = \frac{u_*^2 T_0}{\kappa g \theta_*} \tag{1}$$

where u_* is the friction velocity (ms^{-1}), κ the von Karman constant (generally 0.42 ± 0.01 [9, 11-13]), T_0 the near-ground air temperature (K) and g the gravitational acceleration (9.81 ms^{-2}). The scaling temperature θ_* is given by

$$\theta_* = \frac{-\dot{q}_0}{\rho C_p u_*} \tag{2}$$

where $\dot{q}_0$ is the convective heat flux at the ground surface (Wm^{-2}), which is positive when the corresponding vector is upwards, ρ the air density (kgm^{-3}) and C_p the thermal capacity of air (1006.43 $Jkg^{-1}K^{-1}$). L is positive for stable stratification and negative for unstable stratification [11-14]. Because L is infinite in neutral conditions, in the present work $1/L$ is used to ensure a smooth transition from unstable conditions (negative) over neutral (zero) to stable conditions (positive), and to conveniently associate the MO length L with the Richardson number (Ri). The latter is frequently used to investigate the influence of buoyancy in problems at the scale of individual buildings or that of the urban canopy layer (UCL) or the roughness sublayer (RSL) [15-18].

Although MOST has quite some limitations, such as being an empirical method and a first-order closure to turbulence [9], it is still widely used. It exhibits the advantage that it can describe the vertical profiles of mean streamwise velocity (U), turbulent kinetic energy (TKE, k), turbulence dissipation rate (TDR, ε) and mean temperature (T) as a function of the dimensionless height z/L, and thereby give a complete boundary condition (hereafter referred to as the MOST boundary condition) that can be used for example for computational fluid dynamics (CFD) simulations of non-neutral ABL flow [9,11-14]. However, the actual successful and widespread use of the MOST boundary condition in CFD simulations is still impeded by the challenge of maintaining horizontal homogeneity in those simulations. Horizontal homogeneity implies that the profiles given at the inlet of a computational domain should not show any streamwise gradients while travelling from the inlet of the domain to the position where the objects of interest are located [19-21], when the upstream terrain is uniformly rough and level. In other words, the vertical inlet profiles, the approach-flow profiles and the incident profiles should be the same. Here, the approach-flow profiles are defined as those between the inlet plane and the position where the building model or any other model would be positioned, while the incident profiles are those at the position where the building or any other model would be positioned [19-26]. The vertical profiles of interest are those of U, k, and ε, and in case of non-neutral ABL flow, also temperature T. Horizontal homogeneity is typically tested in an empty computational domain with a level and uniformly rough ground surface [20-23,26].

Essentially, to maintain horizontal homogeneity in the CFD simulation of ABL flow, the boundary conditions, turbulence model and associated model constants must be consistent with one another [19-21]. Following a range of investigations on consistent CFD simulation for neutral conditions [13,19-21,24,27-31], other studies focused on non-neutral conditions. The efforts started by harmonizing the MOST boundary condition and the turbulence model by adding extra source terms in the turbulence model or/and modifying the constants of the

turbulence model [9,11-14]. However, it should be noted that in these previous studies, the proposed source terms always contain the MO length L; and that the turbulence model constants are determined according to the stability at the inlet [9,11-14]. In other words, the potential solutions proposed in these previous studies may be only applicable for the CFD simulations of the stratified ABL over uniformly rough flat terrain and cannot respond to the spatially varying temperature of the practical problem (when there are always irregular terrain topology and/or buildings in the area of interest in the domain), the implementation of these solutions may therefore be limited. A detailed literature review and an illustration on the characteristic of being spatially varying will be provided in the following Section.

The present study aims to provide a new generic and more widely applicable solution that is able to maintain horizontal homogeneity in the CFD modeling of MOST-based stratified ABL flow. This solution should not only maintain the vertical profiles of U, k, ε and T over uniformly rough flat terrain, but also properly respond to the spatially varying temperature and coordinates in practical problems. The remainder of this paper is organized into four sections. Based on a brief introduction to the MOST boundary condition and the governing equations of RANS and the standard k-ε turbulence model, Section 2 presents the derivation of the formulation underlying the new solution. The differences with previous studies are also discussed. The new solution is tested and evaluated for an empty computational domain in Section 3. Section 4 presents the application of the new solution for the CFD simulation of wind flow around a rectangular building under thermal stratification. Section 5 provides the summary and conclusions.

2. Towards a new consistent formulation

2.1. MOST boundary condition

There are various but similar expressions of the MOST inlet boundary condition [10]. The most commonly used expressions adopted in previous studies [9,11-14] are also selected in the present work. The vertical profiles of U, k, ε and T based on MOST are given by:

In stable conditions:

$$U(z) = \frac{u_*}{\kappa}\left(ln\frac{z}{z_0} + 5\frac{z}{L}\right) \tag{3}$$

$$k(z) = \frac{u_*^2}{\sqrt{C_\mu}}\sqrt{\left.1 + 4\frac{z}{L}\right/1 + 5\frac{z}{L}} \tag{4}$$

$$\varepsilon(z) = \frac{u_*^3}{\kappa z}\left(1 + 4\frac{z}{L}\right) \tag{5}$$

$$T(z) = \frac{\theta_*}{\kappa}\left[ln\left(\frac{z}{z_0}\right) + 5\frac{z}{L}\right] + T_0 - \frac{g}{C_p}z \tag{6}$$

In unstable conditions:

$$U(z) = \frac{u_*}{\kappa}\left(ln\frac{z}{z_0} - ln\left[\left(\frac{1+\chi^2}{2}\right)\left(\frac{1+\chi}{2}\right)^2\right] + 2\,arctan\,\chi - \frac{\pi}{2}\right) \tag{7}$$

$$k(z) = \frac{u_*^2}{\sqrt{C_\mu}}\sqrt{\left.1 - \frac{z}{L}\right/\left(1 - 16\frac{z}{L}\right)^{-0.25}} = \frac{u_*^2}{\sqrt{C_\mu}}\sqrt{\chi\left(1 - \frac{z}{L}\right)} \tag{8}$$

$$\varepsilon(z) = \frac{u_*^3}{\kappa z}\left(1 - \frac{z}{L}\right) \tag{9}$$

$$T(z) = \frac{\theta_*}{\kappa}\left[ln\left(\frac{z}{z_0}\right) - 2ln\left(\frac{1+\chi^2}{2}\right)\right] + T_0 - \frac{g}{C_p}z \tag{10}$$

where

$$\chi(z) = \left(1 - 16\frac{z}{L}\right)^{0.25} \tag{11}$$

Note that under neutral conditions, the profiles of U, k and ε are the same to those recommended by Richards and Hoxey [19]:

$$U(z) = \frac{u_*}{\kappa}ln\frac{z}{z_0} \tag{12}$$

$$k(z) = \frac{u_*^2}{\sqrt{C_\mu}} \tag{13}$$

$$\varepsilon(z) = \frac{u_*^3}{\kappa z} \tag{14}$$

$$T(z) = T_0 - \frac{g}{C_p}z \tag{15}$$

Eq. (15) shows that under neutral conditions, the T profile has a gradient (the dry adiabatic lapse

rate) of $\frac{g}{C_p} = \frac{9.81}{1006.43}$ (Km^{-1}). For a horizontally homogeneous ABL flow over uniformly rough flat terrain, when the vertical temperature gradient is greater than the dry adiabatic lapse rate, the atmosphere is in unstable stratification; when the vertical temperature gradient is less than the adiabatic lapse rate, the atmosphere is stable. In most CFD simulations of neutral ABL flow, the energy equation is commonly left out, and temperature variations are thus neglected.

2.2. RANS and the standard *k-ε* equations

In the present work, CFD simulations are carried out using the steady Reynolds-averaged Navier-Stokes (RANS) approach, as it is still widely used for many practical ABL flow problems [32]:

$$\frac{\partial \rho}{\partial t} + \rho \frac{\partial U_i}{\partial x_i} = 0 \tag{16}$$

$$\frac{\partial (\rho U_i)}{\partial t} + \frac{\partial}{\partial x_j}\left(\rho U_i U_j\right) = -\frac{\partial P}{\partial x_i} + \frac{\partial}{\partial x_j}\left[\mu\left(\frac{\partial U_i}{\partial x_j} + \frac{\partial U_j}{\partial x_i}\right) - \overline{u_i u_j}\right] + S_{Mi} \tag{17}$$

$$\frac{\partial (\rho T)}{\partial t} + \frac{\partial}{\partial x_j}\left(\rho T U_j\right) = \frac{\lambda}{C_p} \cdot \frac{\partial}{\partial x_j}\left(\frac{\partial T}{\partial x_j}\right) \tag{18}$$

where S_{Mi} is the source term (kgm^{-2}s^{-2}) and λ the thermal conductivity (Wm^{-1}K^{-1}). The present study assumes that the Reynolds stress terms $\overline{u_i u_j}$ are modeled by the standard *k-ε* turbulence model [33,34]. The corresponding transport equations for *k* and *ε* are:

$$\frac{\partial}{\partial t}(\rho k) + \frac{\partial}{\partial x_j}\left(\rho k U_j\right) = \frac{\partial}{\partial x_j}\left(\frac{\mu_t}{\sigma_k} \cdot \frac{\partial k}{\partial x_j}\right) + G_k - \rho\varepsilon \tag{19}$$

$$\frac{\partial}{\partial t}(\rho \varepsilon) + \frac{\partial}{\partial x_j}\left(\rho \varepsilon U_j\right) = \frac{\partial}{\partial x_j}\left(\frac{\mu_t}{\sigma_\varepsilon} \cdot \frac{\partial \varepsilon}{\partial x_j}\right) + C_{\varepsilon 1}\frac{\varepsilon}{k} G_k - C_{\varepsilon 2}\rho\frac{\varepsilon^2}{k} \tag{20}$$

In Eqs (19) – (20), the time derivative terms are removed in view of steady RANS modeling. In Eqs (19) and (20):

$$\mu_t = \rho C_\mu \frac{k^2}{\varepsilon} \tag{21}$$

$$G_k = \mu_t\left(2 S_{ij} S_{ij}\right) \tag{22}$$

$$S_{ij} = \frac{1}{2}\left(\frac{\partial U_i}{\partial x_j} + \frac{\partial U_j}{\partial x_i}\right) \tag{23}$$

In these equations, μ_t is the turbulent viscosity ($kgm^{-1}s^{-1}$), G_k the production of turbulence kinetic energy due to the mean velocity gradients ($kgm^{-1}s^{-3}$), S_{ij} the strain rate tensor (s^{-1}), and the standard values for the constants are $C_\mu = 0.09$, $C_{\varepsilon 1} = 1.44$, $C_{\varepsilon 2} = 1.92$, $\sigma_k = 1.0$, $\sigma_\varepsilon = 1.3$ [33,34]. When the buoyancy effect is taken into account, the production of k due to buoyancy (G_b) should be added to the right-hand side of the k transport equation (i.e., Eq. (19)). In the CFD simulation of the ABL, G_b is rewritten based on the adiabatic lapse rate [12-14] and given by

$$G_b = -g\frac{\mu_t}{Pr_t}\cdot\frac{1}{T}\cdot\frac{\partial}{\partial z}\left(T + \frac{g}{C_p}z\right) \tag{24}$$

where Pr_t is the turbulent Prandtl number (0.85 in the present work). The term to be added to the ε equation (Eq. (20)) is:

$$C_{\varepsilon 1}C_{\varepsilon 3}\frac{\varepsilon}{k}G_b \tag{25}$$

The definition of $C_{\varepsilon 3}$ is not clear and varies across different CFD software packages. For example, OpenFOAM gives $C_{\varepsilon 3}$ a default value of 0.33 [35]. Whereas in Ansys Fluent 19.0, $C_{\varepsilon 3}$ is calculated by $\tanh\left|\frac{W}{U}\right|$, in which W is the vertical velocity component and U is the horizontal velocity component, assuming the lateral velocity component V is zero [36]. It should be noted that herein U and W are spatially varying, i.e. U and W are expected to be constant at a given height in the empty domain but will be varying when an obstacle is present in the computational domain or in case of unlevel terrain.

For steady RANS simulations with the standard k-ε model of a horizontally homogeneous stratified ABL flow over uniformly rough flat terrain, the following conditions need to apply [19]: (i) the vertical velocity is zero; (ii) the static pressure is constant in the streamwise direction; (iii) the shear stress along the domain length is constant. With these conditions, Eqs. (19) and (20) can be simplified to:

$$\frac{\partial}{\partial z}\left[\left(\frac{\mu_t}{\sigma_k}\right)\frac{\partial k}{\partial z}\right] + G_k + G_b - \rho\varepsilon = 0 \tag{26}$$

$$\frac{\partial}{\partial z}\left[\left(\frac{\mu_t}{\sigma_\varepsilon}\right)\frac{\partial \varepsilon}{\partial z}\right] + C_{\varepsilon 1}\frac{\varepsilon}{k}(G_k + C_{\varepsilon 3}G_b) - C_{\varepsilon 2}\rho\frac{\varepsilon^2}{k} = 0 \tag{27}$$

In the present work, the analytical solution of each term in turbulent transport equations (Eqs. (26) and (27)) is calculated. Starting from neutral conditions (recalling Eqs. (12) – (15), i.e. the MOST boundary condition under neutral conditions), inserting Eqs. (12) – (14) in Eq. (22), the analytical solution of G_k is:

$$G_k = \mu_t \left(\frac{\partial U}{\partial z}\right)^2 = \frac{\rho}{\kappa} \cdot u_*^3 \cdot \frac{1}{z} \tag{28}$$

and $\rho\varepsilon$ is:

$$\rho\varepsilon = \frac{\rho}{\kappa} \cdot u_*^3 \cdot \frac{1}{z} \tag{29}$$

Note that in neutral conditions, inserting Eq. (15) in Eq. (24) yields that the production of k due to buoyancy (G_b, Eq. (24)) is zero, which is:

$$G_b = -g \frac{\mu_t}{Pr_t} \cdot \frac{1}{T} \cdot \frac{\partial}{\partial z}(T_0) = 0 \tag{30}$$

It should be emphasized that Eqs. (12) – (15) only satisfy Eq. (27) if the turbulence model constants ($C_\mu, C_{\varepsilon 1}, C_{\varepsilon 2}, \sigma_\varepsilon$) are determined in such a way that Eq. (31) is satisfied [19,20]:

$$C_{\varepsilon 2} - C_{\varepsilon 1} = \frac{\kappa^2}{\sigma_\varepsilon \cdot \sqrt{C_\mu}} \tag{31}$$

Eq. (31) is also satisfied for the non-neutral conditions investigated in the present work.

For a horizontally homogeneous stratified ABL flow over uniformly rough flat terrain, in stable conditions (recalling Eqs. (3) – (6), i.e. the MOST boundary condition under stable conditions), following the same procedure as above, inserting Eqs. (3) – (5) in Eq. (22), the analytical solution of G_k is:

$$G_k = \mu_t \left(\frac{\partial U}{\partial z}\right)^2 = \frac{\rho}{\kappa} \cdot u_*^3 \cdot \frac{1}{z} \cdot \left(1 + 5\frac{z}{L}\right) \tag{32}$$

and $\rho\varepsilon$ is:

$$\rho\varepsilon = \frac{\rho}{\kappa} \cdot u_*^3 \cdot \frac{1}{z} \cdot \left(1 + 4\frac{z}{L}\right) \tag{33}$$

Inserting Eq. (6) in Eq. (24), the analytical solution of G_b is:

$$G_b = -g\frac{\mu_t}{Pr_t}\cdot\frac{1}{T}\cdot\frac{\partial}{\partial z}\left(T+\frac{g}{C_p}z\right) = -\frac{\rho}{\kappa}\cdot u_*^3\cdot\frac{1}{L} \tag{34}$$

Under stable conditions, G_b is negative and tends to suppress the turbulence [9,11,12].

Note that the ratio of G_b and G_k is the same as the definition of the Ri number, and the analytical solution of the Ri number under stable conditions thus can be obtained, as shown in Eq. (35). The MO length and Ri number are therefore related as follows:

$$Ri = -\frac{g}{\rho}\frac{\partial\rho/\partial z}{\left[\frac{\partial U}{\partial z}+\frac{\partial V}{\partial z}\right]^2} = -\frac{G_b}{G_k} = \frac{\frac{z}{L}}{1+5\frac{z}{L}} \tag{35}$$

where $U\ and\ V$ denote the two horizontal velocity components. According to Eq. (35), the Ri number in stable conditions is positive. Inserting Eqs. (3) – (6) into Eq. (27), the left-hand side of Eq. (27) becomes:

$$\frac{\partial}{\partial y}\left[\left(\frac{\mu_t}{\sigma_\varepsilon}\right)\frac{\partial\varepsilon}{\partial z}\right] + C_{\varepsilon1}\frac{\varepsilon}{k}(G_k + C_{\varepsilon3}G_b) - C_{\varepsilon2}\rho\frac{\varepsilon^2}{k} \approx$$

$$-\frac{1}{\sigma_\varepsilon}\cdot\rho u_*^4\cdot\frac{1}{z^2}\cdot\left\{\left(5\frac{z}{L}\Big/1+5\frac{z}{L}\right)^2 + 5.5\frac{z}{L} + 4.473\left(\frac{z}{L}\right)^2 + \frac{C_{\varepsilon1}C_{\varepsilon3}}{(C_{\varepsilon2}-C_{\varepsilon1})}\cdot\left[\frac{z}{L}+4.5\left(\frac{z}{L}\right)^2\right]\right\} \tag{36}$$

For a horizontally homogeneous ABL flow under stable conditions over uniformly rough flat terrain, Eq. (36) should be zero, $C_{\varepsilon3}$ thus should have the analytical solution described by Eq. (37):

$$C_{\varepsilon3} = \frac{C_{\varepsilon1}-C_{\varepsilon2}}{C_{\varepsilon1}}\cdot\frac{\left(5\frac{z}{L}\Big/1+5\frac{z}{L}\right)^2+5.5\frac{z}{L}+4.473\left(\frac{z}{L}\right)^2}{\frac{z}{L}+4.5\left(\frac{z}{L}\right)^2} \tag{37}$$

In unstable conditions (recalling Eqs. (7) – (11), i.e. the MOST boundary condition under unstable conditions), inserting Eqs. (7) – (9) in Eq. (22), the analytical solution of G_k is:

$$G_k = \mu_\tau\left(\frac{\partial U}{\partial z}\right)^2 = \frac{\rho}{\kappa}\cdot u_*^3\cdot\frac{1}{z\chi} \tag{38}$$

And that of $\rho\varepsilon$ is:

$$\rho\varepsilon = \rho\frac{u_*^3}{\kappa z}\left(1-\frac{z}{L}\right) = \frac{\rho}{\kappa}\cdot u_*^3\cdot\frac{16}{L}\cdot\frac{1}{1-\chi^4} - \frac{\rho}{\kappa}\cdot u_*^3\cdot\frac{1}{L} \tag{39}$$

Inserting Eq. (10) in Eq. (24), the analytic solution of G_b (under unstable conditions) is:

$$G_b = -\frac{\rho}{\kappa} \cdot u_*^3 \cdot \frac{1}{L\chi} \tag{40}$$

Under unstable conditions, G_b is positive and tends to enhance the turbulence [9,11,12].

Note that in neutral and stable conditions, $(G_k + G_b)$ is equal to $\rho\varepsilon$, rendering Eq. (26) satisfied, whereas in unstable conditions, $(G_k + G_b)$ does not equal $\rho\varepsilon$. Although the impact of the term $\frac{\partial}{\partial z}\left[\left(\frac{\mu_t}{\sigma_k}\right)\frac{\partial k}{\partial z}\right]$ under unstable conditions cannot be neglected as is the case in stable conditions, its value still cannot fully cover the discrepancy due to $G_k + G_b - \rho\varepsilon$. In the present work, to cover the discrepancy in Eq. (26) under unstable conditions without changing the corresponding profiles of U, k or T (based on MOST), the ε profile is slightly modified as described in Eq. (41). Following the same procedure of obtaining Eqs (38) and (40), the analytical solutions of G_k and G_b (under unstable conditions) based on the modified ε are as shown in Eqs. (42) and (43).

$$\varepsilon(z) = \frac{u_*^3}{\kappa z}\left(1 - \frac{z}{L}\right) \cdot \chi^{-0.625} \tag{41}$$

$$G_k = \mu_\tau \left(\frac{\partial U}{\partial z}\right)^2 = \frac{\rho}{\kappa} \cdot u_*^3 \cdot \frac{16}{L\chi^{0.375}} \cdot \frac{1}{1-\chi^4} = \frac{\rho}{\kappa} \cdot u_*^3 \cdot \frac{1}{z\chi^{0.375}} \tag{42}$$

$$G_b = -g\frac{\mu_t}{Pr_t} \cdot \frac{1}{T} \cdot \frac{\partial}{\partial z}\left(T + \frac{g}{C_p}z\right) = -\frac{\rho}{\kappa} \cdot u_*^3 \cdot \frac{1}{L\chi^{0.375}} \tag{43}$$

The Ri number, as expressed in Eq. (44), under unstable conditions is negative.

$$Ri = -\frac{G_b}{G_k} = \frac{z}{L} \tag{44}$$

Again, inserting Eqs. (7) – (11) into Eq. (27), the left-hand side of Eq. (27) becomes:

$$\frac{\partial}{\partial y}\left[\left(\frac{\mu_t}{\sigma_\varepsilon}\right)\frac{\partial \varepsilon}{\partial z}\right] + C_{\varepsilon 1}\frac{\varepsilon}{k}(G_k + C_{\varepsilon 3}G_b) - C_{\varepsilon 2}\rho\frac{\varepsilon^2}{k} \approx \frac{1}{\sigma_\varepsilon} \cdot \rho u_*^4 \cdot \frac{1}{z^2} \cdot$$

$$\left[\frac{3\chi+\chi^{-3}}{4} + \frac{(1-\chi^4)^2}{409.6}\left(\frac{45}{\chi^7} - \frac{1}{\chi^3}\right) + \frac{C_{\varepsilon 1}}{C_{\varepsilon 2}-C_{\varepsilon 1}}\left(1-\frac{z}{L}\right)^{0.5}\chi^{-1.5} - \frac{C_{\varepsilon 2}}{C_{\varepsilon 2}-C_{\varepsilon 1}}\left(1-\frac{z}{L}\right)^{1.5}\chi^{-1.75} - \frac{C_{\varepsilon 1}C_{\varepsilon 3}}{(C_{\varepsilon 2}-C_{\varepsilon 1})} \cdot \right.$$

$$\left.\frac{z}{L}\left(1-\frac{z}{L}\right)^{0.5}\chi^{-1.5}\right] \tag{45}$$

Recalling Eq. 11:

$$\chi(z) = \left(1 - 16\frac{z}{L}\right)^{0.25} \tag{11}$$

For a horizontally homogeneous ABL flow under unstable conditions over uniformly rough flat terrain, Eq. (45) should be zero, $C_{\varepsilon 3}$ thus should have an analytical solution described by Eq. (46):

$$C_{\varepsilon 3} = \frac{C_{\varepsilon 1} - C_{\varepsilon 2}}{C_{\varepsilon 1}} \cdot \frac{\frac{3\chi + \chi^{-3}}{4} + \frac{\left(1-\chi^4\right)^2}{409.6}\left(\frac{45}{\chi^7} - \frac{1}{\chi^3}\right) + \frac{C_{\varepsilon 1}}{C_{\varepsilon 2} - C_{\varepsilon 1}}\left(1-\frac{z}{L}\right)^{0.5}\chi^{-1.5} - \frac{C_{\varepsilon 2}}{C_{\varepsilon 2} - C_{\varepsilon 1}}\left(1-\frac{z}{L}\right)^{1.5}\chi^{-1.75}}{-\frac{z}{L}\left(1-\frac{z}{L}\right)^{0.5}\chi^{-1.5}} \tag{46}$$

2.3. Determination of $C_{\varepsilon 3}$

The failure of maintaining horizontal homogeneity is attributed to the incompatibility or inconsistency between the MOST boundary condition and the standard k-ε equations. A tiny deviation at the inlet can grow dramatically along the streamwise direction [20]. In the governing equation for k, the discrepancy can be compensated by rewriting the temperature gradient in G_b based on the dry adiabatic lapse rate, as given by Eq. (24). The discrepancy due to the derivative of $\left(\frac{\mu_t}{\sigma_k}\right)\frac{\partial k}{\partial z}$ has a slight influence under stable conditions; whereas, in unstable conditions, the discrepancy due to the derivative of $\left(\frac{\mu_t}{\sigma_k}\right)\frac{\partial k}{\partial z}$ cannot be ignored, the profile of ε (under unstable conditions) is thus modified, as explained above and described by Eq. (41).

However, how to handle the discrepancy in the ε governing equation is still unclear. Pieterse and Harms [12] tried to achieve horizontal homogeneity in the profiles of mean velocity, turbulence properties and temperature for the stratified ABL flow by modifying the turbulence model constants ($\left(C_\mu, C_{\varepsilon 1}, C_{\varepsilon 2}, \sigma_k, \sigma_\varepsilon\right) = (0.0333, 1.176, 1.92, 1.44, 1.0, 1.3)$) in the ε governing equation. The new model constants still satisfy the relation recommended by Richards and Hoxey [19]. In the governing equation for ε, Pieterse and Harms neglected the influence of the term $\frac{\varepsilon}{k}G_b$ by giving $C_{\varepsilon 3}$ a nil value.

Other studies suggested a $C_{\varepsilon 3}$ depending on the stability at the inlet. The value of $C_{\varepsilon 3}$ suggested by Chang et al. [14] was -0.8 in stable conditions and 0.72 in unstable conditions, whereas Alinot and Masson recommended 3.4 for stable and -4.4 for unstable conditions [9]. Based on the analytical solutions of the simplified turbulent transport equations, Temel and van Beeck gave a more complicated function of $C_{\varepsilon 3}$ as described by Eq. (47) [13]:

$$C_{\varepsilon 3} = \frac{L\phi_m}{\kappa z}_{\varepsilon}[C_{\varepsilon 1}(\phi_m - 1) - C_{\varepsilon 2}(\phi_\varepsilon - 1)] \quad (47)$$

In stable conditions:

$$\phi_m = 1 + 5\frac{z}{L} \quad (48)$$

$$\phi_\varepsilon = 1 + 4\frac{z}{L} \quad (49)$$

In unstable conditions:

$$\phi_m = \left(1 - 16\frac{z}{L}\right)^{-0.25} \quad (50)$$

$$\phi_\varepsilon = 1 - \frac{z}{L} \quad (51)$$

Eqs. (47) – (51) indicate that $C_{\varepsilon 3}$ does not exhibit vertical uniformity, however, the proposed $C_{\varepsilon 3}$ is still a function of the MO length L and the vertical coordinate, indicating that it is dependent on the stability at the inlet. In addition, such coefficient may be only applicable to the CFD simulations of the stratified ABL over uniformly rough flat terrain. In practical problem when there are often irregular terrain topology, buildings, or other obstacles, z or ϕ_ε (in the denominator) may be zero. In short, $C_{\varepsilon 3}$ should be irrespective of the stability at the domain inlet (i.e. $C_{\varepsilon 3}$ should not depend on the MO length L or the vertical coordinate z).

The analytical solutions of $C_{\varepsilon 3}$ obtained in the present work (Eq. (37) for stable conditions and Eq. (46) for unstable conditions) show that for the horizontally homogeneous stratified ABL, the coefficient $C_{\varepsilon 3}$ should always consist of $\frac{C_{\varepsilon 1}-C_{\varepsilon 2}}{C_{\varepsilon 1}}$ and a function of the Ri number. Drawing on the work by Henkes et al. [37] (in their work, $C_{\varepsilon 3}$ is calculated by $\tanh\left|\frac{W}{U}\right|$) and according to the curves as shown in Fig. 1 (two stable and one unstable example conditions are considered in the present work, the corresponding values of L are 152.4 m, 1071.7 m and -296.3 m, respectively), based on a mathematical observation, a hyperbolic function *sech* is selected as such hyperbolic function always has a positive value (no more than 1) for all real numbers, and in addition, has a similar tendency to the curves calculated by Eq. (37) and Eq. (46). The new description of the coefficient $C_{\varepsilon 3}$ then has a form of $\frac{C_{\varepsilon 1}-C_{\varepsilon 2}}{C_{\varepsilon 1}} \cdot A \cdot$

$sech(B \cdot Ri)$. The constants *A* and *B* are determined by curve fitting. This work finally proposes a new description of the coefficient $C_{\varepsilon 3}$ given by

$$C_{\varepsilon 3} = \frac{C_{\varepsilon 1} - C_{\varepsilon 2}}{C_{\varepsilon 1}} \cdot 5.8 \cdot sech(10Ri) \tag{52}$$

The comparison between the coefficient $C_{\varepsilon 3}$ calculated by Eq. (37) (under stable conditions) or Eq. (46) (under unstable conditions) and that by Eq. (52) is shown in Fig. 1. The coefficient $C_{\varepsilon 3}$ proposed in the present work is always negative and has a maximum absolute value of 1.933. Note that the horizontal velocity gradient in Ri is expressed as the algebraic sum of $\partial U/\partial z$ and $\partial V/\partial z$. For a stratified ABL flow over uniformly rough flat terrain, the analytical solution of *Ri* is $5\frac{z}{L} \Big/ 1 + 5\frac{z}{L}$ in stable condition or $\frac{z}{L}$ in unstable condition. It should be emphasized that the *Ri* number in Eq. (52) is spatially varying (based on the spatially varying velocity components and temperature, i.e. are varying in the practical problem) and different from that determined by the MOST boundary condition at the inlet.

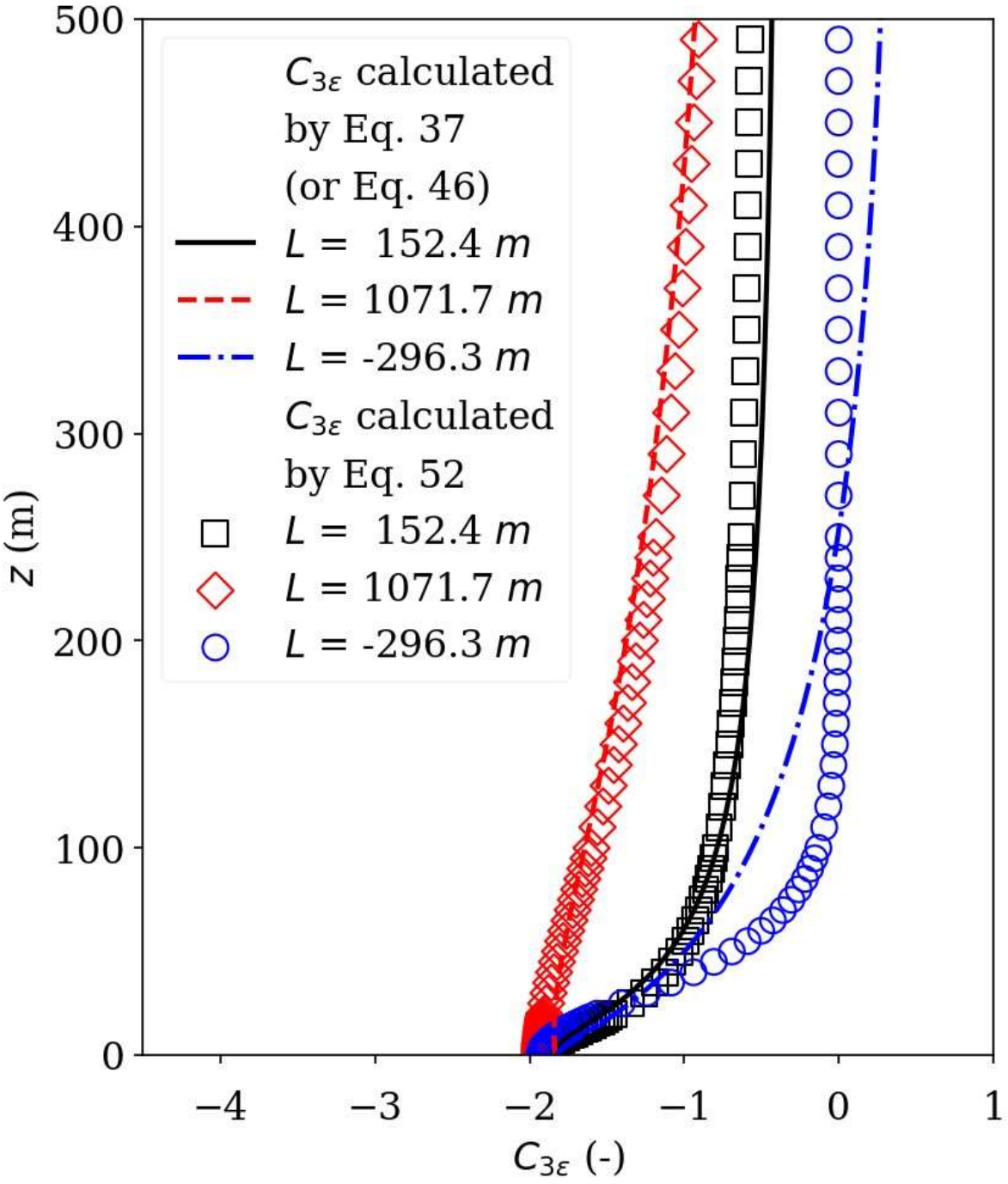

Fig. 1. The comparison of $C_{\varepsilon 3}$ between that calculated by Eq. (37) (under stable condition) or Eq. (46) (under unstable condition) and by Eq. (52).

In the energy equation, a source term should be added due to the use of a compressible fluid [12], which is:

$$S_{Energy} = \frac{\partial}{\partial x_i}\left(-\frac{\mu_t \cdot g}{Pr_t}\right) \tag{53}$$

2.4. Wall roughness for the stratified ABL flow

To maintain horizontal homogeneity in neutral conditions, equations relating the equivalent sand-grain roughness height k_s and the roughness constant C_s to the aerodynamic roughness length z_0 were recommended by Blocken et al. [20]. For Ansys Fluent, this relation is:

$$\frac{k_S C_S}{z_0} = 9.793 \tag{54}$$

It emerges from the momentum wall function in Ansys Fluent, which, when $C_s k_S^+ \gg 1$, is given by [20]:

$$\frac{U_P}{u_*} = \frac{1}{\kappa} ln\left(\frac{u_* z_P}{\upsilon C_S k_S^+}\right) + 5.43 \tag{55}$$

Where the nondimensional roughness height k_S^+ is

$$k_S^+ = u_* k_s / \upsilon \tag{56}$$

More information can be found in Blocken et al. [20]. Following the same procedure, for Eq. (55), a perfect match with Eq. (3) (the mean streamwise velocity under stable conditions) or Eq. (7) (the mean stream-wise velocity under unstable conditions) can be obtained, yielding

$$\frac{k_S C_S}{z_0} = e^{5.43\kappa + \Psi_m(z_P, z_0, L)} \tag{57}$$

Ψ_m depends on the stability of the ABL. In stable conditions:

$$\Psi_m\,(z_P) = \frac{u_*}{\kappa}\left(ln\frac{z_P}{z_0} + 5\frac{z_P}{L}\right) \tag{58}$$

In unstable conditions:

$$\Psi_m\,(z_P) = \frac{u_*}{\kappa}\left(ln\frac{z_P}{z_0} - ln\left[\left(\frac{1+\chi^2}{2}\right)\left(\frac{1+\chi}{2}\right)^2\right] + 2\,arctan\,\chi - \frac{\pi}{2}\right) \tag{59}$$

The value of $\Psi_m(z_P, z_0, L)$ will very slightly affect the actual friction velocity in the wall-adjacent cells. Therefore, the equivalent sand-grain roughness height k_s and the roughness constant C_s recommended by Blocken et al. [20] can still be used.

3. Evaluation of the new formulation in an empty domain

3.1. Computational domain and mesh

The empty 2D computational domain for evaluation of the new formulation is schematically depicted in Fig. 2. Its dimensions are $L_{Domain} \times H_{Domain} = 5000 \times 500$ m². The computational cost is not the prime concern in the horizontal homogeneity tests, the 2D domain is therefore discretized by a structured mesh where the wall-adjacent cells, namely the first layer of cells above the ground surface, have a uniform height of 0.5 m (this cell height is determined through jointly considering the mesh resolution and the effect of wall functions on horizontal homogeneity, further information can be found in [20]). In the vertical direction, the part of the domain below 100 m is divided into 53 intervals, with a growth ratio of 1.04 between adjacent cells and a maximum height of 4.7 m. In the domain above 100 m, the cells have a uniform height of 5 m. In the horizontal direction, the domain is divided into 2500 intervals, with a minimum length of 0.5 m and a maximum length of 5.2 m.

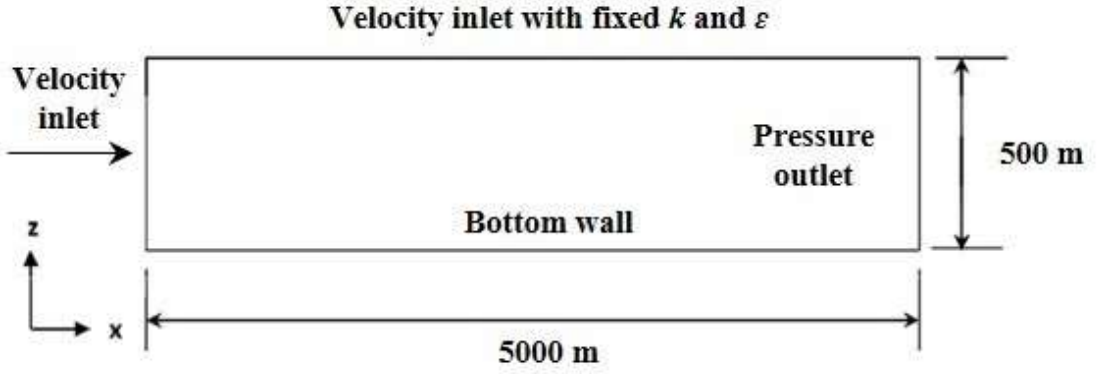

Fig. 2. 2D computational domain and boundary conditions for the horizontal homogeneity test.

3.2. Boundary conditions

The vertical temperature gradient of the dry adiabatic lapse rate under neutral conditions indicates that the compressible ideal gas should be used. Dynamic viscosity, molecular weight,

thermal capacity and thermal conductivity are 1.7894×10^{-5} $kgm^{-1}s^{-1}$, 28.966 $gmol^{-1}$, 1006.43 $Jkg^{-1}K^{-1}$ and 0.0242 $Wm^{-1}K^{-1}$, respectively.

At the inlet, a velocity inlet boundary condition is used, which implies imposing vertical profiles of mean velocity U, turbulence quantities k and ε and temperature T according to Eqs. (3) - (15). The work by Pieterse and Harms [12] is referenced in determining the inlet profiles. Please note that in their work, the reference height was taken as 10 m, whereas in the present work, for the convenience of comparing different stabilities and later modeling of the ABL flow around a rectangular building, a constant reference velocity of 15 ms^{-1} is set at the height of 125 m. Additionally, in the present work, four stability conditions are considered, the corresponding values of $1/L$ are 1/152.4 m^{-1}, 1/1071.7 m^{-1}, 0 m^{-1} and -1/296.3 m^{-1}, respectively.

Because a compressible fluid is being used, a pressure outlet condition is employed at the outlet edge, which means that a static pressure profile is imposed. The pressure profile at the outlet can be obtained from that at the inlet edge after an initial iteration. The flow pattern is found to be very susceptible to the pressure distribution at the outlet. As an alternative solution, a velocity inlet boundary condition can be used at the outlet: only the mean wind speed profile is required, which is the same as that at the inlet. Profiles of k, ε and T can also be added but this is not mandatory. The final static pressure pattern obtained from the two strategies is the same. At the ground surface, the standard wall functions by Launder and Spalding [34] with sandgrain-based roughness modification by Cebeci and Bradshaw [38] are applied. At the top edge, also a velocity inlet boundary condition is imposed with the values of k and ε from the inlet profiles at this specific height (i.e. 500 m) [20,39].

Detailed information on the boundary conditions is listed in Table 1, and the corresponding Pasquill classes [40] are also given. The profiles at the inlet for the four stabilities are shown in Fig. 3.

Table 1

All investigated cases.

u_* (m s^{-1})	U_{ref} (m s^{-1})	z_0 (m)	k_s (m)	C_s (-)	$\dot{q}_0$ (W m^{-2})	T_0 (K)	$1/L$ (m^{-1})	Stability	Pasquill class
0.464	15.00	0.01	0.196	0.5	-57.0	298.15	$\frac{1}{152.4}$	Stable	E
0.627					-20.0		$\frac{1}{1071.7}$	Stable	E
0.666					0.0		0	Neutral	D
0.721					110.0		$\frac{-1}{296.3}$	Unstable	C

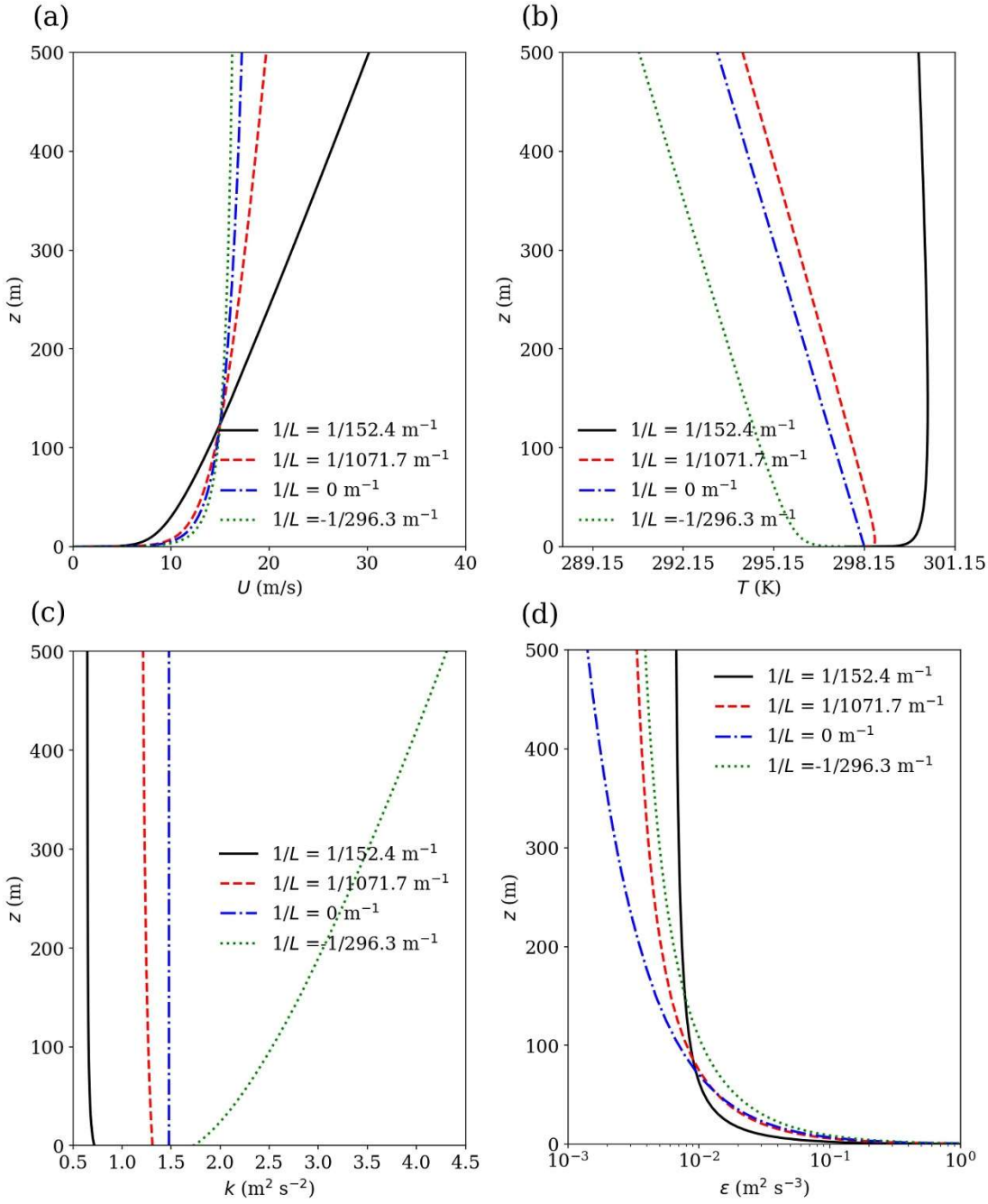

Fig. 3. Inlet profiles under four investigated thermal stratifications a) U; b) T; c) k; d) ε.

3.3. Other numerical settings

The 2D steady RANS equations are solved with the standard k-ε model for closure. The

solver is Ansys Fluent 19.0. Pressure is discretized with the body force weighted scheme; other properties are discretized with second-order upwind schemes. As the compressible fluid and extra source terms are introduced, the Coupled method is used for coupling pressure and velocity. The scaled residuals are used to judge convergence; they are set at 1×10^{-6}.

3.4. Results and error analysis

To judge horizontal homogeneity, the vertical profiles at the inlet, 100 m, 500 m, 1000 m, 2500 m and 5000 m are compared (Fig. 4a-d – 7a-d). According to Eq. (60), where φ_{inlet} denotes U, k, ε or T at the inlet and φ_x denotes the corresponding variable at a specific place in the domain downstream of the inlet, errors at 2 m and 20 m height are calculated and they are shown in Fig. 4e – 7e.

$$error = 100 \cdot \left| \frac{\varphi_x - \varphi_{inlet}}{\varphi_{inlet}} \right| \tag{60}$$

The deviations of U, k, ε and T are given in Table A1. Although the errors are not zero, the profiles of U, ε and T are nevertheless well maintained; only the k profiles exhibit some minor deviations, but for all tested stabilities, the errors of k at heights of 2 m and 20 m are no more than 5%; while for the stable and neutral conditions, these k errors are less than 2% for the entire computational domain, as shown in Fig. 4e – 7e.

The remaining errors may be attributed to: (i) the discretization schemes of the software; (ii) the discrepancy in the governing equation of k (Eq. (26)) due to the term $\frac{\partial}{\partial z}\left[\left(\frac{\mu_t}{\sigma_k}\right)\frac{\partial k}{\partial z}\right]$, especially in unstable conditions; (iii) the discrepancy in the governing equation for ε (Eq. (27)), which is not perfectly covered by the buoyancy term with the proposed $C_{\varepsilon 3}$.

The values of k in the near-wall region also exhibit a slight oscillation but within a minimal range; the values of k are not always larger or smaller than that at the inlet, which suggests that there is no major inconsistency between the MOST boundary condition and the modified standard k-ε turbulence model but the software's discretization strategy or algorithm may result in the inhomogeneity; otherwise the deviation would be expected to grow as the profiles travel through the domain.

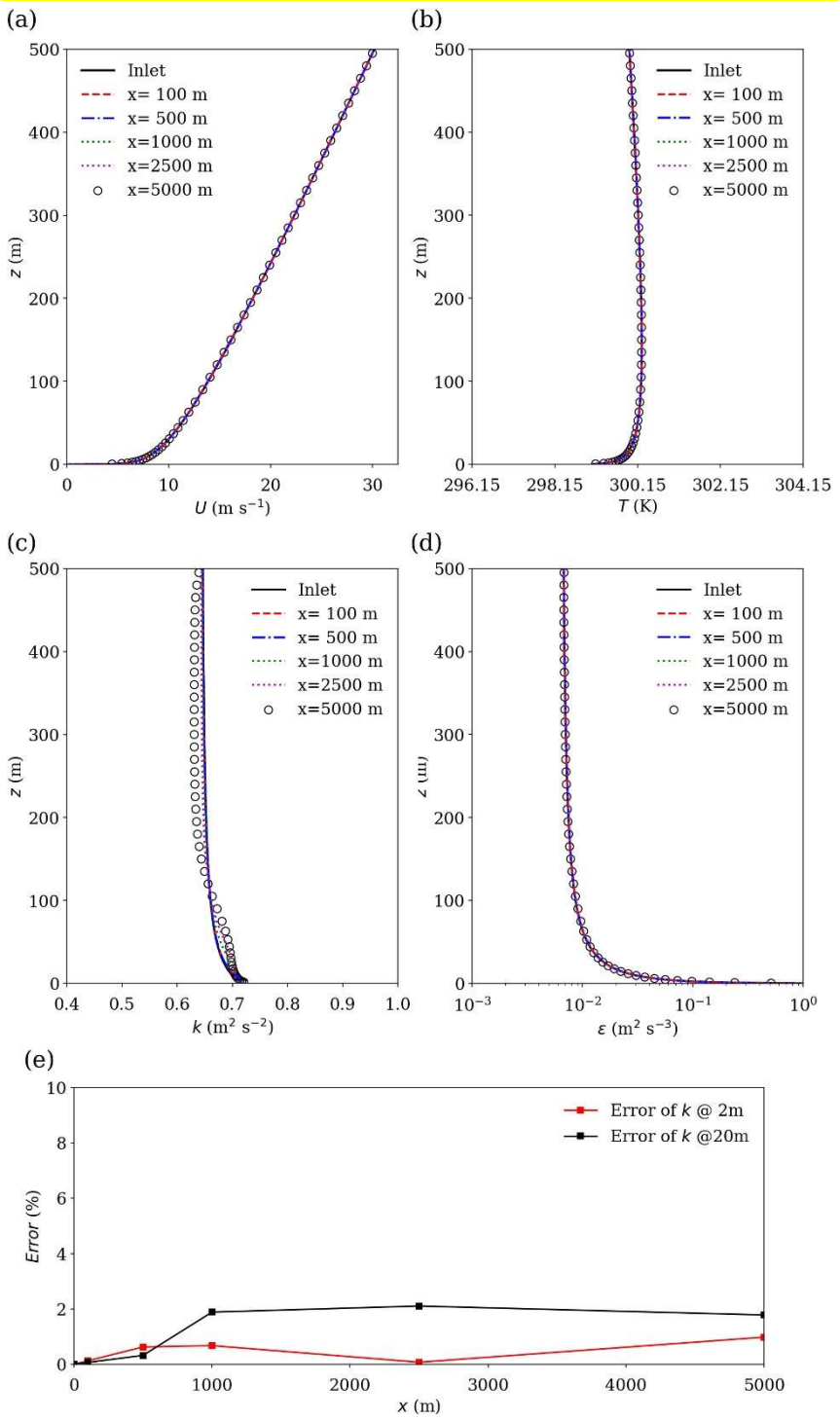

Fig. 4. Comparison of vertical profiles under the stable condition $1/L = 1/152.4$ m^{-1}: a) U; b) T; c) k; d) ε; e) errors of k at 2 m and 20 m height.

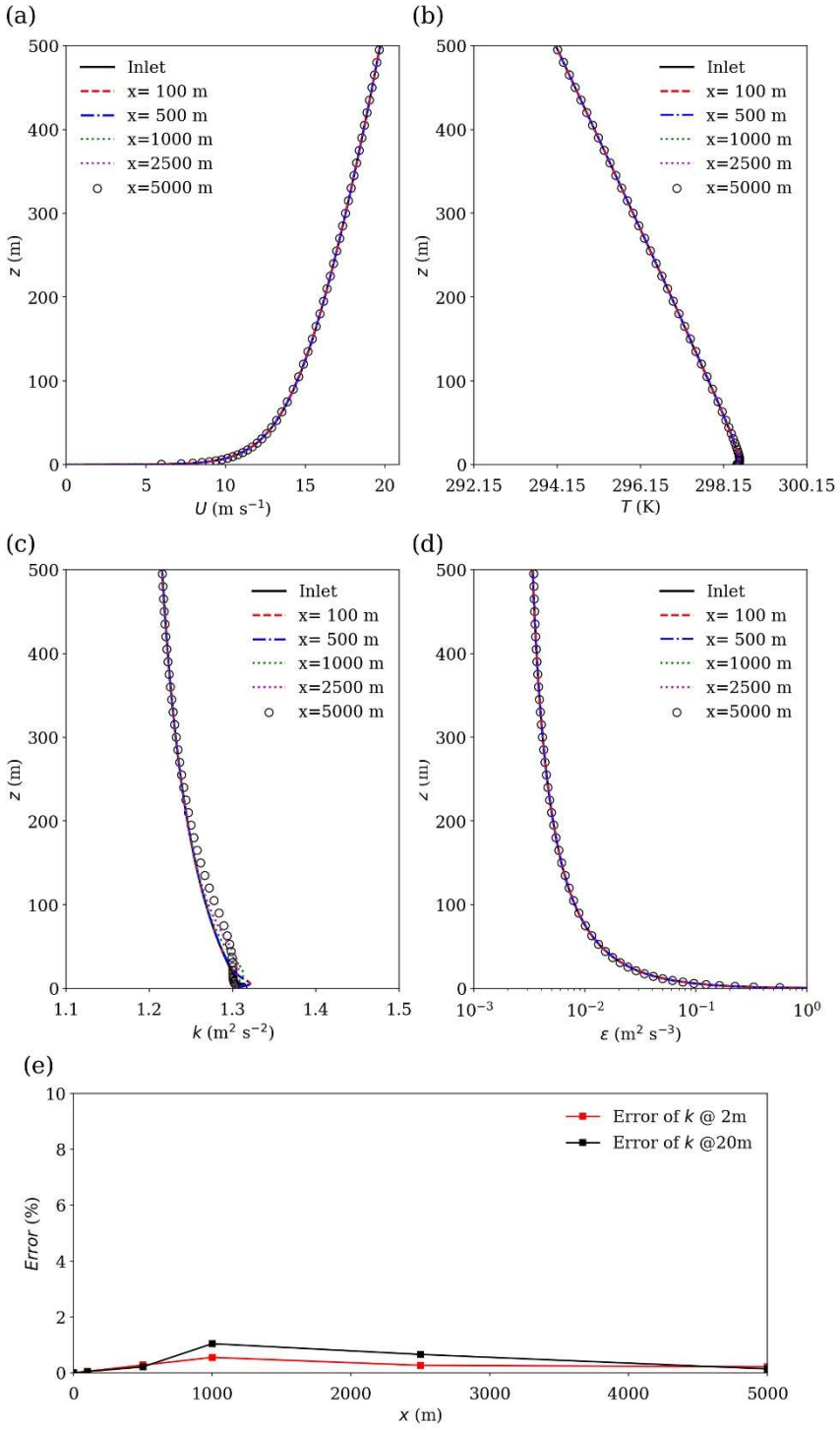

Fig. 5. Comparison of vertical profiles under the stable condition $1/L = 1/1071.7$ m^{-1}: a) U; b) T; c) k; d) ε; e) errors of k at 2 m and 20 m height.

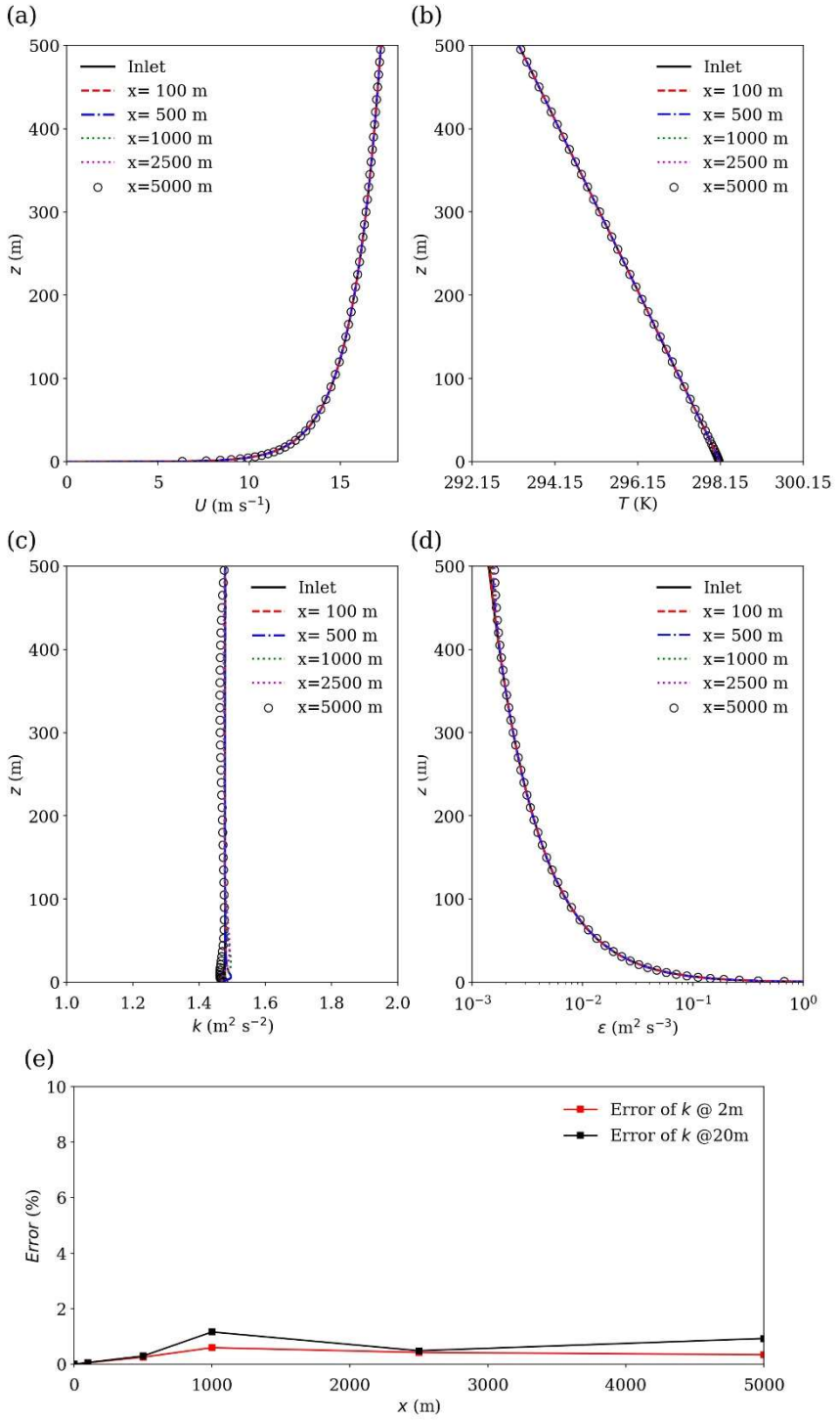

Fig. 6. Comparison of vertical profiles under the neutral condition $1/L = 0$ m^{-1}: a) U; b) T; c) k; d) ε; e) errors of k at 2 m and 20 m height.

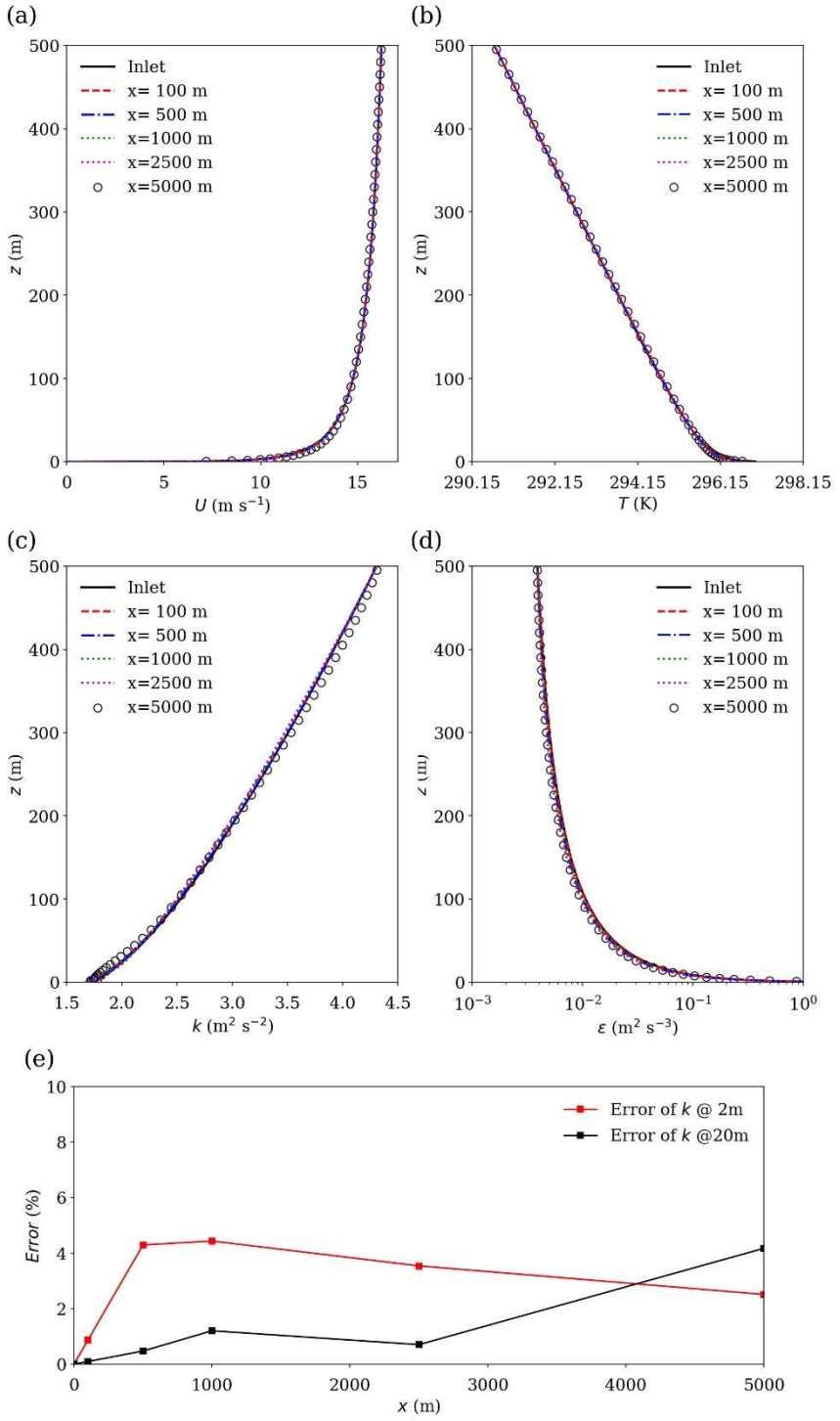

Fig. 7. Comparison of vertical profiles under the unstable condition $1/L$ = -1/296.3 m^{-1}: a) U; b) T; c) k; d) ε; e) errors of k at 2 m and 20 m height.

4. Evaluation of the new formulation for wind flow around an isolated rectangular building

4.1. Computational domain, mesh and other settings

As discussed before, adding a new term in the turbulence model equations (i.e. the equation for ε in the present work) brings about a potential clash in practical CFD simulations, especially when there is the presence of an obstacle and/or a vertical temperature gradient (although in the coefficient $C_{\varepsilon 3}$ proposed in the present work, all variables are spatially varying). Therefore, the flow around a rectangular building under thermal stratification is further studied in the present work. The rectangular building will act as the obstacle. Along with the separation, reattachment, stagnation and recirculation of the flow around the building, the vertical temperature gradient around the building is also subject to change.

(a)

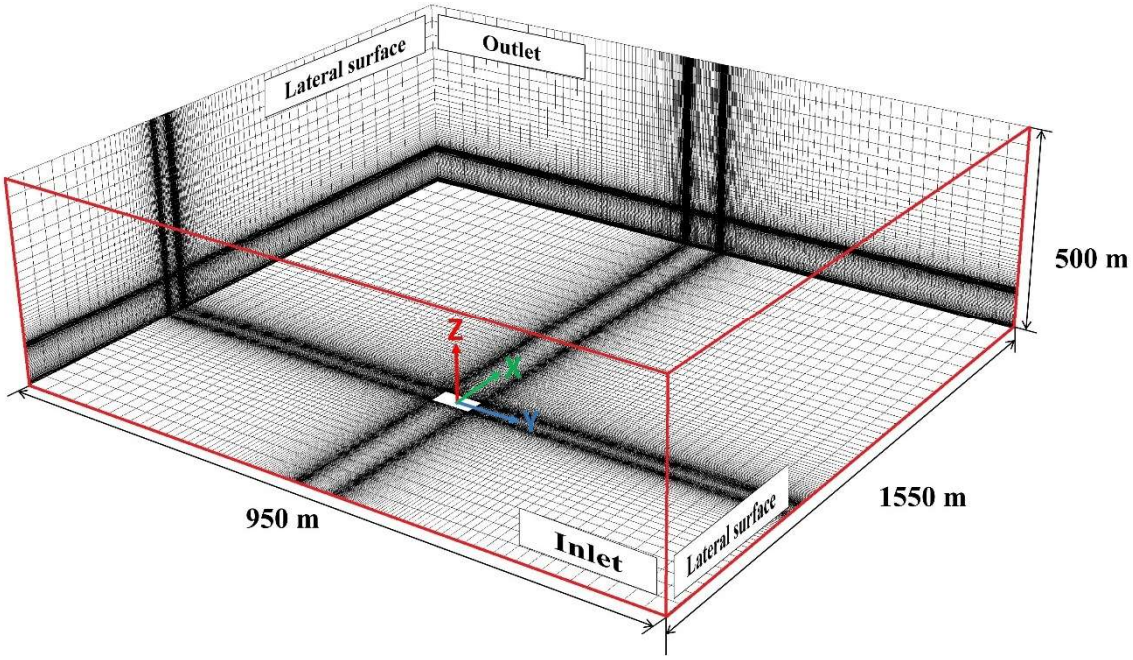

(b)

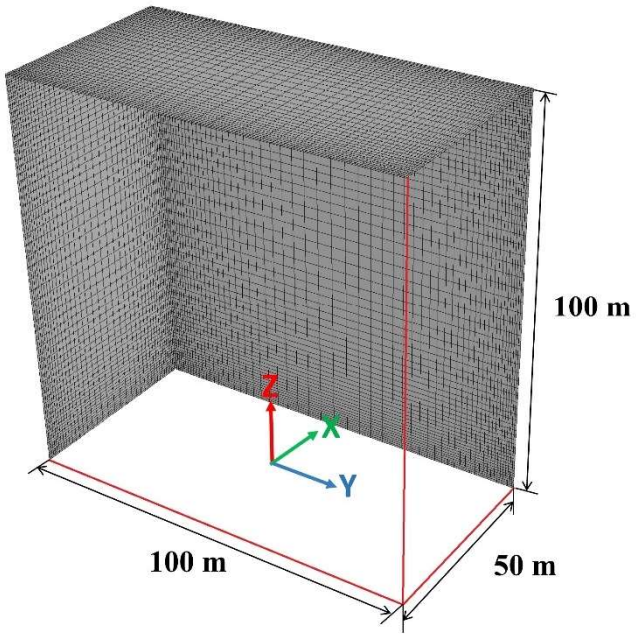

Fig. 8. 3D computational domain and computational grid on the building surfaces and on the ground, lateral and back faces of the domain.

The 3D computational domain and mesh are established based on the best practice guidelines [41, 42]. The computational domain has dimensions 1550 m (length) × 950 m (width) × 500 m (height), as shown in Fig. 8(a). The building has dimensions 50 m (length) × 100 m (width) × 100 m (height, H). It is positioned at 500 m from the inlet, as shown in Fig. 8(b). The Cartesian coordinate system is defined with the origin at the building bottom. A completely structured mesh is built: the mesh is extruded from the bottom surface; the wall-adjacent cells, namely the first layer of cells to the bottom, have a uniform normal height of 0.5 m; the first layer of cells normal to the building surfaces has a uniform normal height of 0.2 m; the mesh at the height of 200 m is particularly refined with a size of 0.2 m. The growth ratio between adjacent cells (in all three directions) is no more than 1.1. The total number of cells is 6,378,960.

The four degrees of stability used in Section 3 (1/152.4 m^{-1}, 1/1071.7 m^{-1}, 0 m^{-1} and -1/296.3 m^{-1}) are also applied here. The boundary conditions at the inlet, outlet, top and bottom surfaces are the same as in Section 3. The pressure distribution at the pressure outlet surface is obtained as in Section 3. Periodic boundary conditions are employed at the lateral surfaces of the domain. Building surfaces are set to be adiabatic. Detailed boundary conditions are listed

in Table 1. The standard k-ε model with the new $C_{\varepsilon 3}$ is used. The code for the ε source term with the new $C_{\varepsilon 3}$ is presented in Appendix B, please note that this code is strongly subject to the CFD software package. The other numerical settings including discretization schemes are the same as those in Section 3. For all variables, the scaled residuals used to judge convergence are set at 1×10^{-6}.

4.2. Results and discussion

The flow fields in the XZ plane (y = 0.0) under the four investigated stabilities are shown in Fig. 9. The most obvious difference lies in the downstream area of the building: as the stability varies from stable over neutral to unstable, the recirculation region exhibits a decreasing tendency.

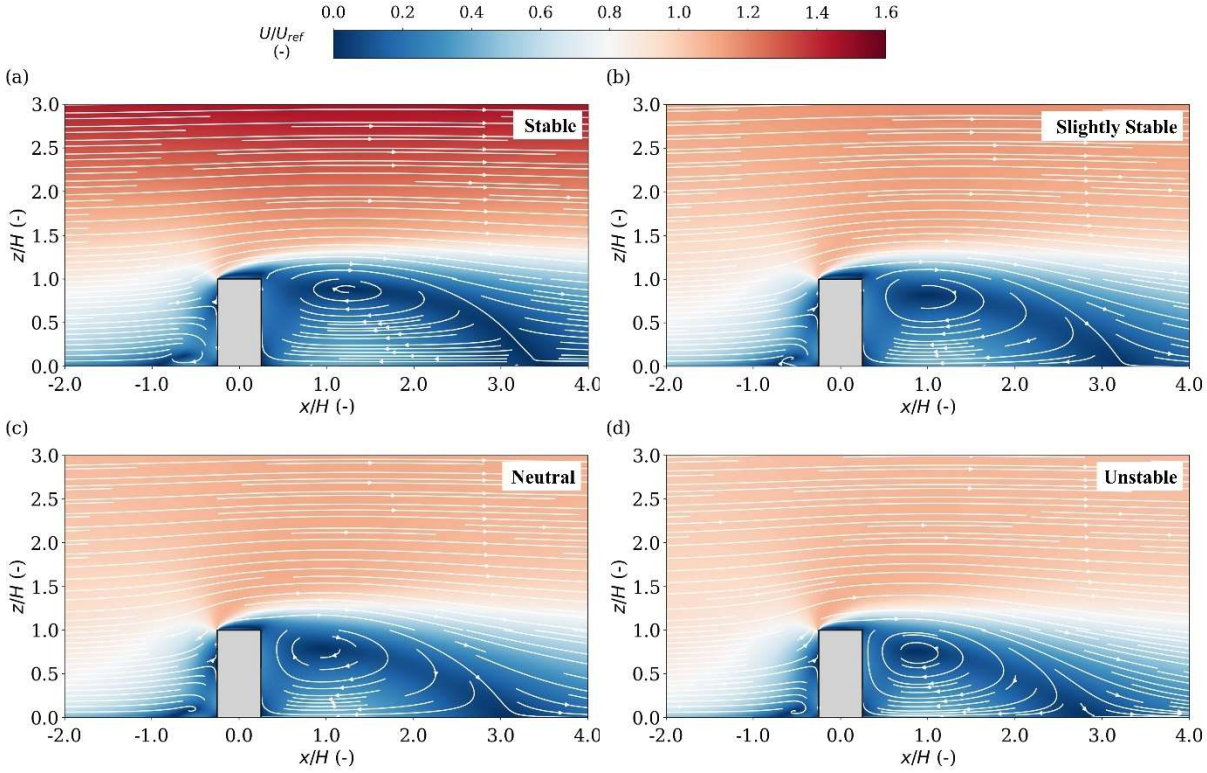

Fig. 9. Contours of normalized velocity in the vertical centerplane under a) $1/L$ = 1/152.4 m^{-1}; b) $1/L$ = 1/1071.7 m^{-1}; c) $1/L$ = 0 m^{-1}; d) $1/L$ = -1/296.3 m^{-1}.

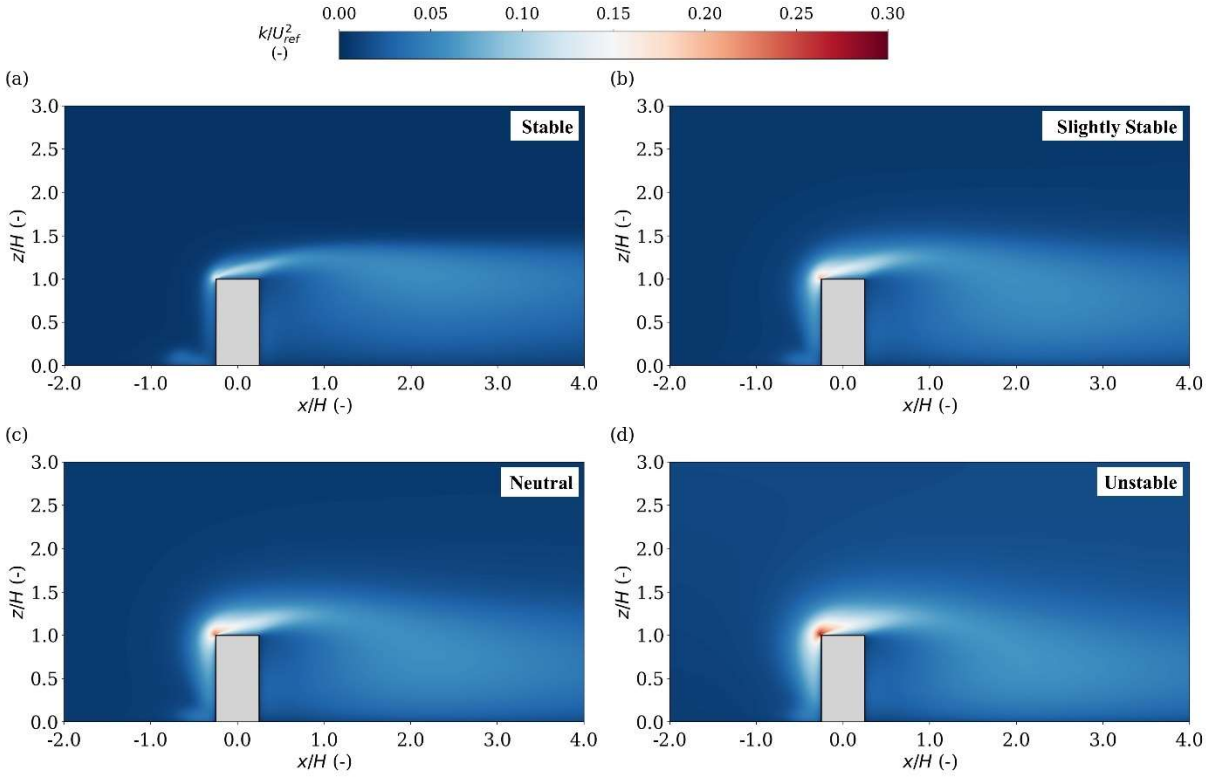

Fig. 10. Contours of normalized turbulent kinetic energy in the vertical centerplane under a) $1/L$ = 1/152.4 m^{-1}; b) $1/L$ = 1/1071.7 m^{-1}; c) $1/L$ = 0 m^{-1}; d) $1/L$ = -1/296.3 m^{-1}.

For the k fields, as the unstable condition investigated in the present work has a larger value of k at the inlet, especially in the higher region (recalling Fig. 3(c)), the largest normalized k is identified in the unstable condition. However, under stable conditions, due to the higher velocity gradient in the vertical direction, the normalized k above and behind the building can also have a similar magnitude as that in the unstable condition, as shown in Fig. 10. The maximum k always appears at the leading edge of the building.

The relative temperatures $T - T_0$ are shown in Fig. 11, where T_0 is the near-ground air temperature. As the background temperature in the strongly stable condition is more uniform, a separate color bar is employed here, whereas the other three cases share a color bar ranging from -1 to 5 K. The building's leeward edge always sees a higher temperature due to the entrainment of warmer air. To better illustrate how the presence of a building influences the temperature field under different thermal stratifications, the temperature variations under the four stabilities are compared in Fig. 12 in terms of T - T_{inlet} where T_{inlet} depends on the stability and the vertical coordinate z. Such a temperature field is mainly decided by the mixture of the

air at different heights. For the slightly stable, neutral and unstable conditions (in which the airflow at a higher level is cooler than that at a lower level; see Fig. 3), in the front of the building, due to the downward cooler air flow, negative variations of (T - T_{inlet}) can be identified around the windward surface of the building at the pedestrian-level; the downstream of the building can also see negative variations of (T - T_{inlet}) due to the vortex; while the positive variations around the building's leeward leading edge can be attributed to the upward warmer airflow from the lower level. Such a tendency is more pronounced when the stability varies from slightly stable over neutral to unstable as shown in Fig. 12(b) – (d). The temperature pattern in the case of the strongly stable condition is different because the flow temperature is more uniform at its inlet (see Fig. 3(b)), and the variations around the building and in the building's downstream are generally positive due to the downward warmer airflow (as shown in Fig. 12(a)). Note that the positive variation means that the temperature is higher than the temperature of the same level at the inlet but does not imply that the flow is heated.

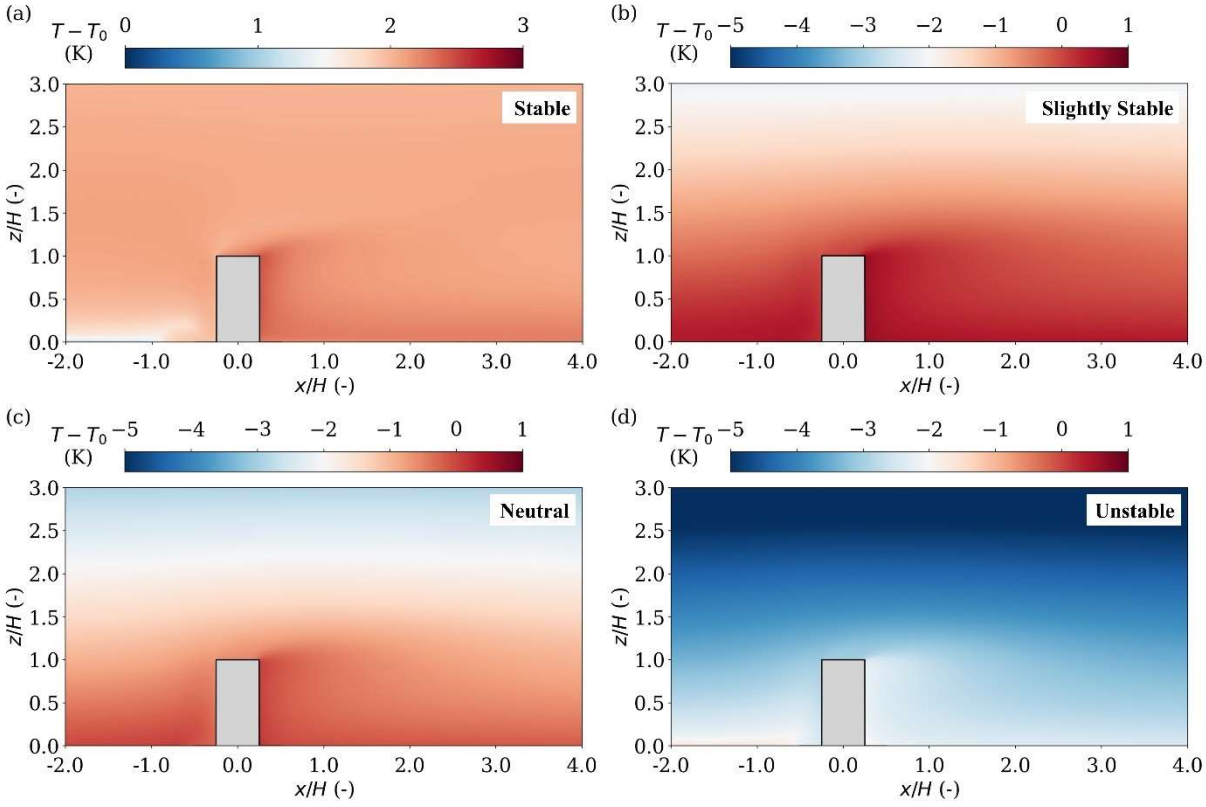

Fig. 11. Contours of relative temperature in the vertical centerplane under a) $1/L$ = 1/152.4 m^{-1}; b) $1/L$ = 1/1071.7 m^{-1}; c) $1/L$ = 0 m^{-1}; d) $1/L$ = -1/296.3 m^{-1}.

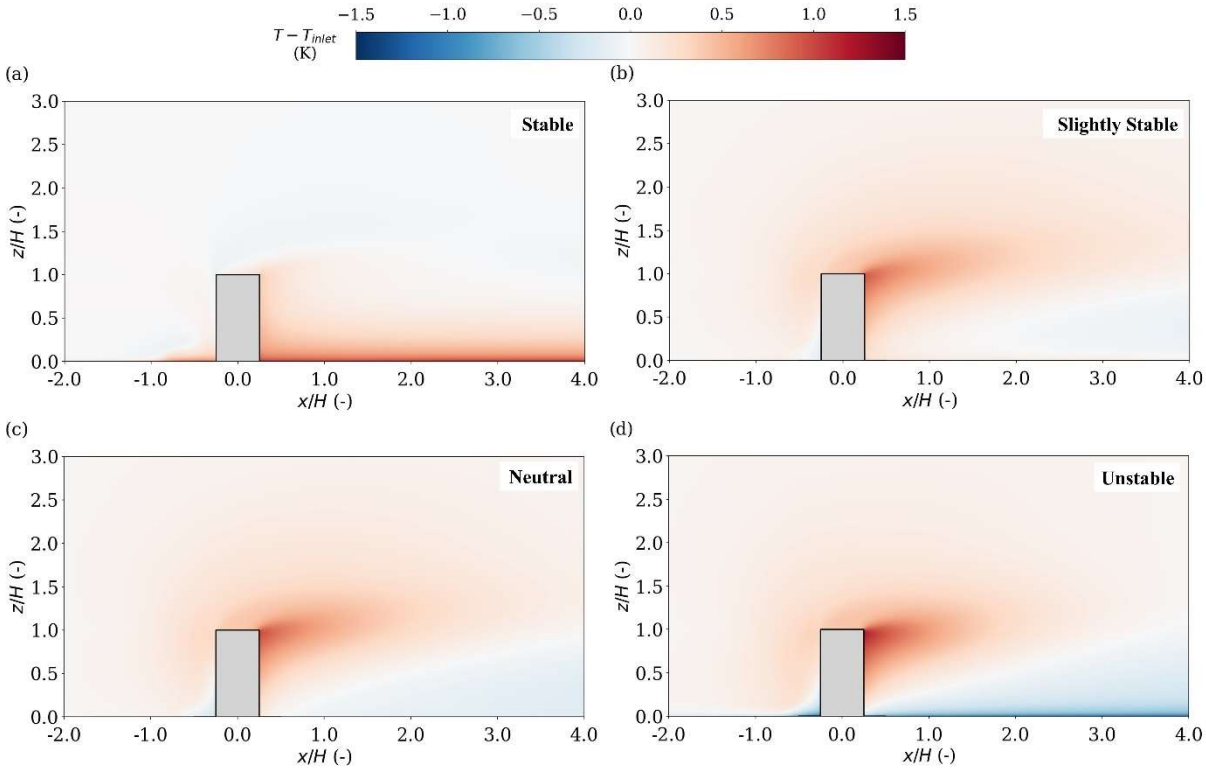

Fig. 12. Contours of temperature difference in the vertical centerplane under a) $1/L$ = 1/152.4 m^{-1}; b) $1/L$ = 1/1071.7 m^{-1}; c) $1/L$ = 0 m^{-1}; d) $1/L$ = -1/296.3 m^{-1}.

Fig. 9 and Fig. 11 also show that the velocity components (in streamwise and vertical directions) and temperature are spatially varying due to the presence of the building, the resultant $C_{\varepsilon 3}$ is spatially varying too, but not like that determined by the stability at the domain inlet. It should be emphasized again that the modeling of the flow around the rectangular building is to check if the standard k-ε with proposed $C_{\varepsilon 3}$ can respond to the obstacle and variable temperature gradient in the incident region. The modeling results do not show apparent conflict.

5. Summary and conclusions

This paper aims to provide a generic and more widely applicable solution to maintain

horizontal homogeneity in the CFD modeling of MOST-based stratified ABL flow. This solution should not only maintain the vertical profiles of U, k, ε and T over uniformly rough flat terrain, but also properly respond to the spatially varying temperature and coordinates in practical problems. The contributions to obtain this objective are summarized as follows:

- The ε profile under unstable conditions is modified.
- For the stratified ABL over uniformly rough flat terrain, the analytical solutions of G_b (the production of k due to buoyancy) are $-\frac{\rho}{\kappa}\cdot u_*^3\cdot\frac{1}{L}$ under stable conditions and $-\frac{\rho}{\kappa}\cdot u_*^3\cdot\frac{1}{L\chi}$ under unstable conditions.
- For the stratified ABL over uniformly rough flat terrain, the analytical solutions of the Ri number are $\frac{z}{L}\Big/1+5\frac{z}{L}$ in stable conditions and $\frac{z}{L}$ in unstable conditions.
- The discrepancy in the governing equation for ε, which is the main reason for the failure to maintain horizontal homogeneity under thermal stratification, is explicitly calculated for stable and unstable conditions.

This paper finally proposes a new description of the coefficient $C_{\varepsilon 3}$, which appears in the buoyancy term in the ε equation. Horizontal homogeneity tests are first conducted in an empty computational domain for four stability conditions (covering all three stabilities, the corresponding values of $1/L$ are 1/152.4 m^{-1}, 1/1071.7 m^{-1}, 0 m^{-1} and -1/296.3 m^{-1}, respectively). In conclusion, the standard k-ε turbulence model with the new $C_{\varepsilon 3}$ can well maintain the profiles of U, ε and T while only the k profiles observe minor deviations. For all tested stabilities, the errors of k at heights of 2 m and 20 m are not larger than 5%, while for stable and neutral conditions, the errors of k are lower than 2%. The performance of the proposed solution is also successfully demonstrated by modeling the flow around a rectangular building under thermal stratification.

The consistency problem between Monin-Obukhov similarity theory and the standard k-ε model results in the failure to maintain horizontal homogeneity for the CFD simulation of the stratified ABL. Nevertheless, this inconsistency also indicates that the standard k-ε model with previous treatments of $C_{\varepsilon 3}$ may be unable to correctly predict the MOST-based stratified ABL since the correct velocity and turbulence properties within the computational domain should be the numerical solution to the governing equations of k and ε, whereas, for the MOST-based stratified ABL, this requirement cannot be satisfied even for the most ideal and simplified case of uniformly rough flat terrain. From this perspective, this work proposes a potential solution.

To maintain horizontal homogeneity, the MOST boundary condition and the standard k-ε model are made consistent by a mathematical derivation. Minor consistency discrepancies still persist, resulting in deviations, especially in the k profiles. Further and future modifications can still be made in $C_{\varepsilon 3}$ or in the buoyancy term in the governing equations for k and ε, but for these additional theoretical analyses are required.

Acknowledgements

The author would like to thank the anonymous reviewers for their valuable comments and suggestions.

The work described in this paper was supported by the General Research Grant from the Research Grants Council of the Hong Kong Special Administrative Region, China (Project No. CityU 11217722). The CFD simulations conducted in the present work were supported by the National Supercomputer Center in Guangzhou, China.

Appendix A

Table A1

Deviations of U, k, ε and T in the horizontal homogeneity tests.

			100 m	500 m	1000 m	2500 m	5000 m
$1/L$ = 1/152.4 m^{-1}	U (ms^{-1})	z = 2 m	0.03	0.05	0.09	0.11	0.13
		z = 20 m	-0.01	-0.01	-0.02	0.00	0.03
	T (K)	z = 2 m	0.01	0.01	0.02	0.03	0.03
		z = 20 m	0.00	0.00	0.00	0.01	0.01
	k (m^{2}s^{-2})	z = 2 m	0.00	-0.01	-0.01	-0.00	0.01
		z = 20 m	0.00	0.00	0.01	0.01	0.01
	ε	z = 2 m	0.00	-0.01	-0.01	-0.00	0.00

	(m^2s^{-3})	z = 20 m	0.00	0.00	0.00	0.00	0.00
$1/L$ = 1/1071.7 m^{-1}	U	z = 2 m	0.02	0.03	0.05	0.10	0.16
	(ms^{-1})	z = 20 m	-0.02	-0.02	-0.02	0.00	0.04
	T	z = 2 m	0.00	0.01	0.02	0.03	0.03
	(K)	z = 20 m	0.00	0.00	0.00	0.01	0.01
	k	z = 2 m	0.00	0.00	0.01	0.00	0.00
	(m^2s^{-2})	z = 20 m	0.00	0.00	0.01	0.00	0.00
	ε	z = 2 m	-0.01	-0.01	-0.01	0.00	0.00
	(m^2s^{-3})	z = 20 m	0.00	0.00	0.00	0.00	0.00
$1/L$ = 0 m^{-1}	U	z = 2 m	0.04	0.05	0.05	0.08	0.12
	(ms^{-1})	z = 20 m	-0.02	-0.01	-0.01	0.00	0.03
	T	z = 2 m	0.00	0.00	-0.01	-0.02	-0.03
	(K)	z = 20 m	0.00	0.00	0.00	0.00	0.00
	k	z = 2 m	0.00	0.00	-0.01	0.01	-0.01
	(m^2s^{-2})	z = 20 m	0.00	0.00	0.01	0.01	-0.01
	ε	z = 2 m	-0.02	-0.02	-0.01	-0.01	-0.01
	(m^2s^{-3})	z = 20 m	0.00	0.00	0.00	0.00	0.00
$1/L$ = -1/296.3 m^{-1}	U	z = 2 m	0.05	0.08	0.12	0.15	0.18
	(ms^{-1})	z = 20 m	-0.02	0.02	0.02	0.06	0.10
	T	z = 2 m	-0.05	-0.11	-0.12	-0.13	-0.13
	(K)	z = 20 m	0.01	0.00	-0.01	-0.02	-0.01
	k	z = 2 m	-0.01	-0.06	-0.07	-0.05	-0.04
	(m^2s^{-2})	z = 20 m	0.00	-0.01	0.02	0.01	0.06
	ε	z = 2 m	-0.04	-0.02	-0.01	-0.01	-0.01
	(m^2s^{-3})	z = 20 m	0.00	0.00	0.00	0.00	0.00

Appendix B

```
DEFINE_SOURCE(TED_source_buoyancy, c, t, dS, eqn)
{
  real source;
  real mut = C_MU_T(c,t);
  real tke = C_K(c,t);
  real ted = C_D(c,t);
  real Gb;

  real t_gradient = C_T_RG(c,t)[VER];
   /* returns the temperature gradient in vertical direction */
  real du_dy = C_U_RG(c,t)[VER];
  real dv_dy = C_W_RG(c,t)[VER];
  real Ri;

  Gb = -9.81*mut*(t_gradient + 9.81/1006.43)/(T_ref);
   Ri = -9.81*(t_gradient + 9.81/1006.43)/(T_ref*(du_dy + dv_dy)*(du_dy + dv_dy));
  source = (5.8/cosh(10*Ri))*ted*(Gb/tke)*(1.44-1.92);
   /* the source term is a bit different from Eq. 52 as Ansys Fluent has another manner */
   dS[eqn] = (5.8/cosh(Ri))*(Gb/tke)*(1.44-1.92);
  return source;
}
```

References

[1] R. Stull, An introduction to boundary layer meteorology, 1988.

[2] P. Drobinski, P. Carlotti, R.K. Newsom, R.M. Banta, R.C. Foster, J.-L. Redelsperger, The structure of the near-neutral atmospheric surface layer, J. Atmos. Sci. 61 (2004).

[3] L. Mahrt, Stably stratified atmospheric boundary layers, Annu Rev Fluid Mech 46 (2014) 23–45. https://doi.org/10.1146/annurev-fluid-010313-141354.

[4] E. Gramsch, D. Cáceres, P. Oyola, F. Reyes, Y. Vásquez, M.A. Rubio, G. Sánchez, Influence of surface and subsidence thermal inversion on PM2.5 and black carbon concentration, Atmos. Environ. 98 (2014) 290–298. https://doi.org/10.1016/j.atmosenv.2014.08.066.

[5] M. Tabib, A. Rasheed, T. Kvamsdal, Investigation of the impact of wakes and stratification on the performance of an onshore wind farm, Energy Procedia. 80 (2015) 301-311. https://doi.org/10.1016/j.egypro.2015.11.434.

[6] W. Wang, B. Chen, Y. Xu, W. Zhou, X. Wang, Urban heat islands in Hong Kong: Bonding with atmospheric stability, Atmos. Sci. Lett. 22 (2021). https://doi.org/10.1002/asl.1032.

[7] A.S. Monin, A.M. Obukhov, Basic laws of turbulent mixing in the surface layer of the atmosphere, Tr. Akad. Nauk SSSR Geophiz. Inst. 24 (1954) 163–187.

[8] A.M. Obukhov, Turbulence in an atmosphere with non-uniform temperature, Boundary-Layer Meteorol. 2 (1971) 7–29.

[9] C. Alinot, C. Masson, *k*-ε model for the atmospheric boundary layer under various thermal stratifications, J. Sol. Energy Eng. 127 (2005) 438-443. https://doi.org/10.1115/1.2035704.

[10] T. Foken, 50 Years of the Monin – Obukhov Similarity Theory, Boundary-Layer Meteorol. 119 (2006) 431–447. https://doi.org/10.1007/s10546-006-9048-6.

[11] M. Pontiggia, M. Derudi, V. Busini, R. Rota, Hazardous gas dispersion: A CFD model accounting for atmospheric stability classes, J. Hazard. Mater. 171 (2009) 739–747. https://doi.org/10.1016/j.jhazmat.2009.06.064.

[12] J.E. Pieterse, T.M. Harms, CFD investigation of the atmospheric boundary layer under different thermal stability conditions, J. Wind Eng. Ind. Aerodyn. 121 (2013) 82–97.

https://doi.org/10.1016/j.jweia.2013.07.014.

[13] O. Temel, J. van Beeck, Two-equation eddy viscosity models based on the Monin – Obukhov similarity theory, Appl. Math. Model. 42 (2017) 1–16. https://doi.org/10.1016/j.apm.2016.09.024.

[14] C. Chang, J. Schmidt, D. Martin, B. Stoevesandt, A consistent steady state CFD simulation method for stratified atmospheric boundary layer flows, J. Wind Eng. Ind. Aerodyn. 172 (2018) 55–67. https://doi.org/10.1016/j.jweia.2017.10.003.

[15] K. Uehara, S. Murakami, S. Oikawa, S. Wakamatsu, Wind tunnel experiments on how thermal stratification affects flow in and above urban street canyons, Atmos. Environ. 34 (2000) 1553–1562. https://doi.org/10.1016/S1352-2310(99)00410-0.

[16] Z.-T. Xie, I.P. Castro, Large-eddy simulation for flow and dispersion in urban streets, Atmos. Environ. 43 (2009) 2174–2185. https://doi.org/10.1016/j.atmosenv.2009.01.016.

[17] A.B. Norton, K. Bosomworth, A. Coutts, N. Williams, S. Livesley, Planning for a cooler future : Green infrastructure to reduce urban heat, October 2013 Climate Adaptation for Decision-makers, 2013.

[18] V.B.L. Boppana, Z.-T. Xie, I.P. Castro, Thermal stratification effects on flow over a generic urban canopy, Boundary-Layer Meteorol. 153 (2014) 141–162. https://doi.org/10.1007/s10546-014-9935-1.

[19] P.J. Richards, R.P. Hoxey, Appropriate boundary conditions for computational wind engineering models using the *k*-*ε* turbulence model, J. Wind Eng. Ind. Aerodyn. 46–47 (1993) 145–153. https://doi.org/http://dx.doi.org/10.1016/0167-6105(93)90124-7.

[20] B. Blocken, T. Stathopoulos, J. Carmeliet, CFD simulation of the atmospheric boundary layer: wall function problems, Atmos. Environ. 41 (2007) 238–252. https://doi.org/10.1016/j.atmosenv.2006.08.019.

[21] B. Blocken, J. Carmeliet, T. Stathopoulos, CFD evaluation of wind speed conditions in passages between parallel buildings—effect of wall-function roughness modifications for the atmospheric boundary layer flow, J. Wind Eng. Ind. Aerod. 95 (2007) 941–962. https://doi.org/10.1016/j.jweia.2007.01.013.

[22] D.M. Hargreaves, N.G. Wright, On the use of the *k*-*ε* model in commercial CFD software to model the neutral atmospheric boundary layer, J. Wind Eng. Ind. Aerodyn.

95 (2007) 355–369. https://doi.org/10.1016/j.jweia.2006.08.002.

[23] B. Blocken, P. Moonen, T. Stathopoulos, J. Carmeliet, Numerical study on the existence of the venturi effect in passages between perpendicular buildings, J. Eng. Mech. 134 (12) (2008) 1021–1028. https://doi.org/10.1061/(ASCE)0733-9399(2008)134:12(1021).

[24] B. Blocken, J. Carmeliet, Pedestrian wind conditions at outdoor platforms in a high-rise apartment building: generic sub-configuration validation, wind comfort assessment and uncertainty issues, Wind Struct. 11 (1) (2008) 51–70. https://doi.org/10.12989/was.2008.11.1.051.

[25] B. Blocken, C. Gualtieri, Ten iterative steps for model development and evaluation applied to Computational Fluid Dynamics for Environmental Fluid Mechanics, Environ. Model. Softw. 33 (2012) 1–22. https://doi.org/10.1016/j.envsoft.2012.02.001.

[26] B. Blocken, Computational Fluid Dynamics for urban physics : Importance, scales, possibilities , limitations and ten tips and tricks towards accurate and reliable simulations, Build. Environ. 91 (2015) 219–245. https://doi.org/10.1016/j.buildenv.2015.02.015.

[27] C. Gorlé, J. van Beeck, P. Rambaud, G. van Tendeloo, CFD modelling of small particle dispersion: The influence of the turbulence kinetic energy in the atmospheric boundary layer, Atmos. Environ. 43 (2009) 673–681. https://doi.org/10.1016/j.atmosenv.2008.09.060.

[28] A. Parente, C. Gorlé, J. van Beeck, C. Benocci, A comprehensive modelling approach for the neutral atmospheric boundary layer: Consistent inflow conditions, wall Function and turbulence model, Boundary-Layer Meteorol. 140 (2011) 411–428. https://doi.org/10.1007/s10546-011-9621-5.

[29] A. Parente, C. Gorlé, J. van Beeck, C. Benocci, Improved k-ε model and wall function formulation for the RANS simulation of ABL flows, J. Wind Eng. Ind. Aerodyn. 99 (2011) 267–278. https://doi.org/10.1016/j.jweia.2010.12.017.

[30] M. Balogh, A. Parente, C. Benocci, RANS simulation of ABL flow over complex terrains applying an Enhanced k-ε model and wall function formulation: implementation and comparison for fluent and OpenFOAM, J. Wind Eng. Ind. Aerod. 104–106 (2012) 360–368. https://doi.org/10.1016/j.jweia.2012.02.023.

[31] M. Balogh, A. Parente, Realistic boundary conditions for the simulation of atmospheric

boundary layer flows using an improved k-ε model, J. Wind Eng. Ind. Aerod. 144 (2015) 183-190. https://doi.org/10.1016/j.jweia.2015.01.010.

[32] B. Blocken, LES over RANS in building simulation for outdoor and indoor applications: A foregone conclusion?, Build. Simul. 11 (2018) 821–870. https://doi.org/10.1007/s12273-018-0459-3.

[33] W. Jones, B.E. Launder, The prediction of laminarization with a two-equation model of turbulence, Int. J. Heat Mass Transf. 15 (1972) 301–314. https://doi.org/10.1016/0017-9310(72)90076-2.

[34] B.E. Launder, D.B. Spalding, The numerical computation of turbulent flows, Comput. Methods Appl. Mech. Eng. 3 (1974) 269–289. https://doi.org/10.1016/0045-7825(74)90029-2.

[35] C.J. Greenshields, OpenFOAM user guide, 2021.

[36] Ansys Inc., Ansys Fluent User's Guide, 15317 (2013) 724–746.

[37] R.A.W.M. Henkes, F.F. van der Vlugt, C.J. Hoogendoorn, Natural-convection flow in a square cavity calculated with low-Reynolds-number turbulence models, Int. J. Heat Mass Transf. 34 (1991) 377–388. https://doi.org/10.1016/0017-9310(91)90258-G.

[38] T. Cebeci, P. Bradshaw, Momentum transfer in boundary layers, 1977.

[39] Y. Toparlar, B. Blocken, B. Maiheu, G.J. van Heijst, CFD simulation of the near-neutral atmospheric boundary layer: New temperature inlet profile consistent with wall functions, J. Wind Eng. Ind. Aerodyn. 191 (2019) 91–102. https://doi.org/10.1016/j.jweia.2019.05.016.

[40] F. Pasquill, F.B. Smith, The physical and meteorological basis for the estimation of the dispersion of windborne material: les bases physiques et meteorologiques pour l'evaluation de la dispersion de matieres portees par le vent, Proc. Second Int. Clean Air Congr. (1971) 1067–1072. https://doi.org/10.1016/B978-0-12-239450-8.50190-8.

[41] J. Franke, A. Hellsten, H. Schlunzen, B. Carissimo, Best practice guideline for the CFD simulation of flows in the urban environment, 2007.

[42] Y. Tominaga, A. Mochida, R. Yoshie, AIJ guidelines for practical applications of CFD to pedestrian wind environment around buildings, J. Wind Eng. Ind. Aerodyn. 96 (2008) 1749–1761. https://doi.org/10.1016/j.jweia.2008.02.058.